General Disclaimer

One or more of the Following Statements may affect this Document

- This document has been reproduced from the best copy furnished by the organizational source. It is being released in the interest of making available as much information as possible.

- This document may contain data, which exceeds the sheet parameters. It was furnished in this condition by the organizational source and is the best copy available.

- This document may contain tone-on-tone or color graphs, charts and/or pictures, which have been reproduced in black and white.

- This document is paginated as submitted by the original source.

- Portions of this document are not fully legible due to the historical nature of some of the material. However, it is the best reproduction available from the original submission.

NATIONAL AERONAUTICS AND SPACE ADMINISTRATION

Technical Memorandum 33-802

Wind Power Prediction Models

JET PROPULSION LABORATORY
CALIFORNIA INSTITUTE OF TECHNOLOGY
PASADENA, CALIFORNIA

November 15, 1976

PREFACE

The work described in this report was performed by the Telecommunications Division of the Jet Propulsion Laboratory.

ACKNOWLEDGEMENT

CONTENTS

ABSTRACT

This report describes investigations performed for the prediction of
the power available from the wind at the Goldstone, California, antenna site
complex. The background for power prediction is derived from a statistical
evaluation of available wind speed data records at this location and at nearby
locations similarly situated within the Mojave Desert. In addition to a
model for power prediction over relatively long periods of time, the report
describes an interim simulation model that produces sample wind speeds.
The interim model furnishes uncorrelated sample speeds at hourly intervals
that reproduce the statistical wind distribution at Goldstone. Beyond this,
there is a discussion of a stochastic simulation model to provide speed samples
representative of both the statistical speed distributions and correlations.

I. INTRODUCTION

The original purpose of the wind model studies was to examine the suitability of the Goldstone site for the collection of wind energy. The specific objectives were to be able to identify promising candidate windmill sites and estimate the incident wind energy. Subsequently, during the evolution of a comprehensive energy system simulation, an additional requirement arose to derive a wind speed simulation model. Consequently, there are two distinct types of models that have been initiated: the original site-evaluation type of model is an attempt to parameterize candidate windmill sites on the basis of relatively long time periods (months or years) for the collection of wind energy; the more recent simulation model attempts to provide sequences of representative sample wind speeds at relatively short time intervals (possibly hours). Although both models evolve from the same basis of the available or projected statistical characteristics of the site, their formulation and application, which tend toward being deterministic in the first case and stochastic in the second, are greatly different. Aside from developing a limited interim model for wind speed simulation and discussion of a proposed extended simulation model, most of the effort to date has been on the original parameter type site evaluation model.

At the start of this program, there was a limited amount of digitized wind speed data available for the Goldstone site. This data had been collected during the years 1966-1968 at three different anemometer heights on a wind tower near the Mars antenna to determine structure wind loading. The records consist of average wind speeds over 5-min periods at sampling intervals of either 1 or 3 hours. There are numerous gaps in the data, because of either the scheduling of the collection program or instrument malfunction. The extent of the data is summarized in Table 1. The anemometers used for data collection were MRI[1] model 1053 vector vanes, which consist of a propeller-type anemometer mounted on a 2-axis (azimuth and elevation) frame. This instrument supplies the wind direction angles and the resultant wind speeds.

The Mars tower is situated on flat, desertlike terrain bordered by a few low hills. This area has some similarities to a typical airport. Consequently, to have supplementary regional data for a better description of local wind phenomena, a substantial amount of U.S. Weather Bureau archive wind speed records were digitized for our computer examination. These consisted of hourly average wind speed records at three nearby airports: Edwards Air Force Base, George Air Force Base and the Daggett Marine Center airport. All of these sites are in the Mojave Desert, as is Goldstone, and within a 110-km (70-mile) radius. Table 2 summarizes the extent of the additional data. The instrumentation used to collect the data and the sampling procedure are not known. The data, however, is supposed to represent the hourly average wind speed determined from a sample of duration of a few minutes or else of an instantaneous estimate by on-site operating personnel.

---

[1]Meteorology Research Inc., 464 West Woodbury Rd., Altadena, CA 91001.

Table 1. Goldstone Mars site available
wind data records

Year	Month	Sampling interval; hr	Anemometer height					
			15 m (50 ft)		46 m (150 ft)		91 m (300 ft)	
			No. of samples	% missing	No. of samples	% missing	No. of samples	% missing
1966	9	1	630	12.5	616	14.4	663	7.9
	10	1	721	3.1	711	4.4	722	3.0
	11	1	704	2.2	703	2.4	703	2.4
	12	3	245	1.2	246	0.8	53	78.6
1967	1	3	210	15.3	245	1.2	0	100.0
	2	3	210	6.2	110	50.9	149	33.5
	3	3	207	16.5	244	1.6	243	2.0
	4	3	237	1.2	238	0.8	239	0.4
	5	3	242	2.4	243	2.0	239	3.6
	6	3	225	6.2	117	51.2	229	4.6
	7	3	197	20.6	197	20.6	188	24.2
	8	3	247	0.4	246	0.8	244	1.6
	9	3	25	89.6	25	89.6	25	89.6
	10		0	100.0	0	100.0	0	100.0
	11	1			390	45.8		
	12	1			703	5.5		
1968	1	1			505	32.1		
	2	1			592	14.9		
	3	1			555	25.4		
	4	1			593	17.7		
	5	1			532	28.5		
	6	1			544	24.5		
	7	1			294	60.5		
	8	1			412	44.6		
	9	1			712	1.1		
	10	1			656	11.8		
Totals			4100		10,429		3697	

Table 2.   Supplementary wind data records

Site	Distance to MARS tower, km	miles	Years From	To	Anemometer ht, m	ft	Sampling interval hours	No. of samples
George AFB	103	64	1951	1955	24.3	80	1	43,746
Daggett	64	40	1962	1964	6.1	20	1	26,280
Marine Ctr.			1965	1973	6.1	20	3	26,280
Edward AFB	109	68	1950	1954	9.8	32	1	43,781
			1957	1970	4.0	13	1	172,709
							Total	262,796

In addition to the older existing data, a new data collection program for the Goldstone site was initiated in October 1974 with 10 anemometers distributed at six sites. Since that date, these have been providing continuous strip chart readings of wind speeds. However, only a relatively small part of this data has currently been reduced to a form suitable for processing. Table 3 provides a summary of the characteristics of these anemometer locations, which incorporate MRI model 1022 wind set equipment. This equipment consists of a cup-type anemometer that measures the horizontal component of wind speed and a vane-type wind azimuth direction indicator. Meteorology Research Inc. assisted in site reconnaissance for these stations and designed, supplied, and erected the instrumentation.

Figure 1 shows the geographical locations of these sites. The China Lake Naval Station site shown was originally expected to provide supplementary regional data. However, since it was found that only daytime recordings of wind speeds were available here, the incomplete China Lake data was not processed. Figure 2 contains a larger-scale map of the Goldstone anemometer sites.

Table 3. Goldstone sites for wind speed data collection

Site	Anemometer ht, m	ft	Comments
1	46	150	MARS site tower, used in 1966-68.
	91	300	
2	10	33	On peak of hill. High wind speeds antici-pated.
	30.5	100	
3	10	33	In flat region. Selected for favorably accessible windmill location.
	30.5	100	
4	30.5	100	At the airport. Selected for comparison with other airport sites.
5	10	33	On peak of ridge. High wind speeds antici-pated.
	30.5	100	
6	30.5	100	On hill. High wind speeds anticipated and also near a relatively large area that could be developed for several windmills.

CHINA LAKE

SITE 001 AT GOLDSTONE MARS

003• •002
005• •004
•006

EDWARDS AFB

DAGGETT

GEORGE AFB
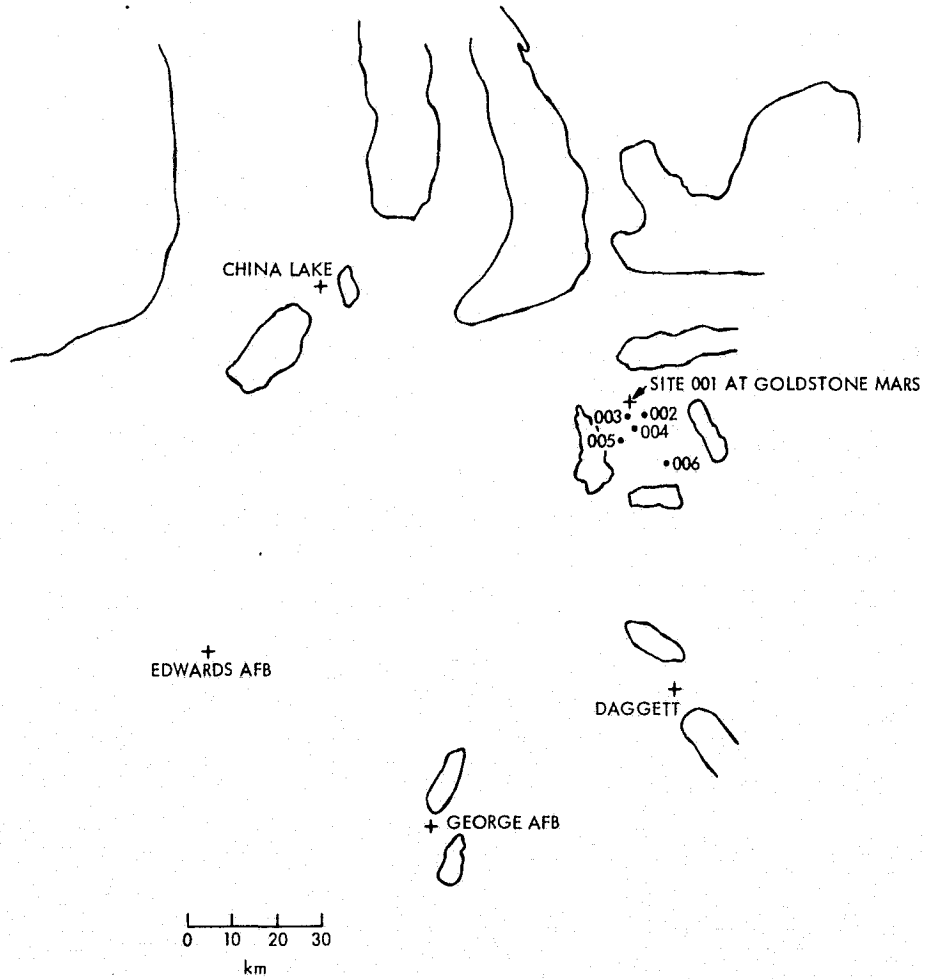
0   10   20   30
km

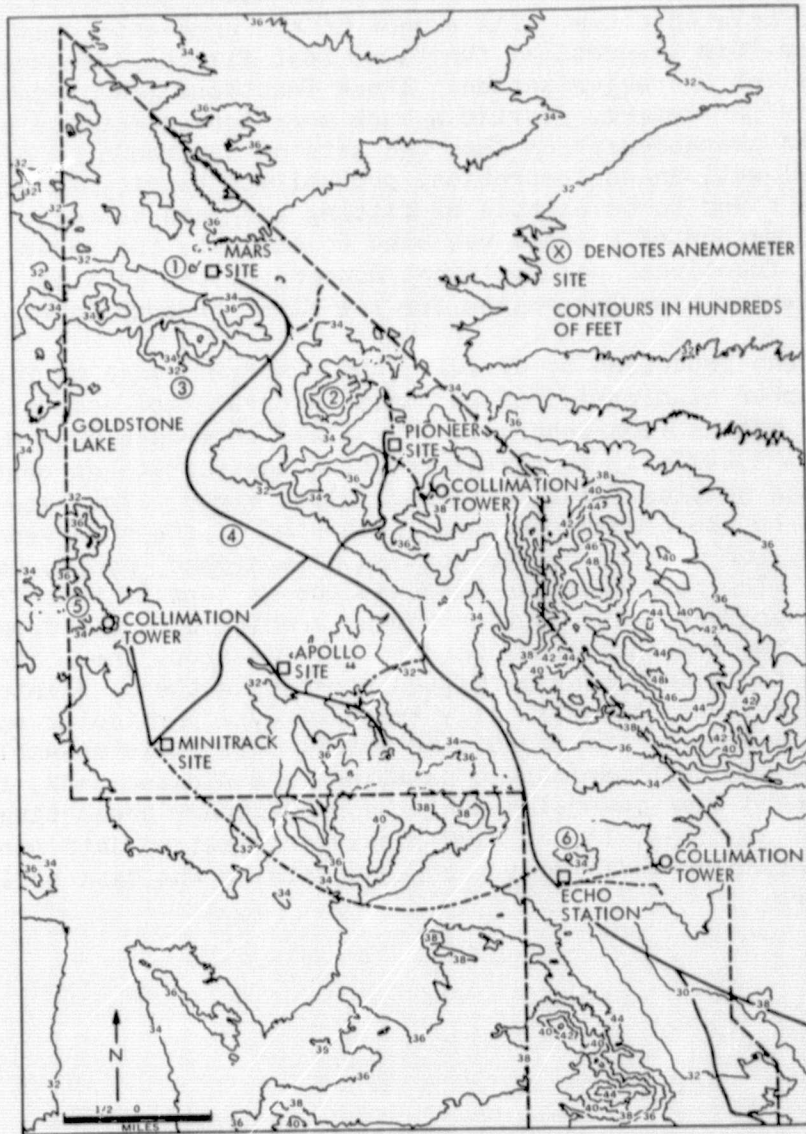Fig. 1.   Location of wind data sites

Fig. 2. Goldstone anemometer sites

II. WIND SPEED DISTRIBUTIONS

A.   DATA PROCESSING

All of the data of Tables 1 and 2 was processed by computer to determine the nature of the conventional wind speed probability densities and distributions[2] at these related sites. One aspect of the processing was to attempt to define closed-form theoretical functions that fit the data approximately for more convenient characterization. These functions, in conjunction with their associated parameters, provide a much more convenient and concise description of the wind characteristics than the sets of thousands of original data values. Several well-known theoretical probability density functions were tested and were found to be capable of fitting the data closely. Since, in general, the method of moments was used to estimate the parameters of the theoretical functions, the empirical moments of the data about the origin and about the center were determined for the first through fourth orders.

The data was processed by dividing the observed range of wind speeds into a large number of closely spaced class intervals and computing the number of observations within each interval. The class intervals used were sufficiently small (1.0 mph = 0.447 m/s) to permit treating the results as continuous data, rather than as classified, with negligible error. The data records that were input to the computer program consisted of the observed wind speed (miles per hour) and a coded representation of the year, month, day and hour of observation. The raw Goldstone data was put on tape in this format by an in-house JPL project. The weather bureau archive data was formatted this way on tapes by our subcontractor, Meteorology Research, Inc. The time code associated with the wind speeds permitted processing the data into subsets of data pools that could be optionally selected over particular spans of days, months or years. As processed, the actual data pools assembled ranged in size from the smallest periods, consisting of a single month, to the largest pools that extended over several years. By preliminary presorting of the data within special files, it was also possible to set up data pools that consisted of particular individual months comprising the data collected from a number of years.

---

[2]Distributions of the random variable x, which we take to include wind speeds, are conventionally characterized by the probability density function $f(x)$, or the probability distribution function (cumulative distribution) $F(x)$. The probability density function is defined so that the probability that the random variable lies within the interval $(x, x+dx)$ is $f(x) dx$. The distribution function $F(x)$ is the probability that the random variable is less than x. For a continuous random variable, $F(x)$ can be computed as the integral of $f(u) du$, where the lower limit of integration extends to the smallest realizable value of the random variable and the upper limit is x.

B. EMPIRICAL DISTRIBUTIONS AND FITTING FUNCTIONS

The wind speed density functions of all the data were typically found to be skewed to the left, with the highest probabilities at the lower speeds and a rapid decay in probability with increasing speed. The median wind speeds were usually from 10 to 20% less than the mean speeds. The standard deviations of the speeds also tended to be considerably less than the mean speeds, but were usually at least half of the mean and occasionally slightly more than the mean.

Although plots of the empirical densities always showed substantial irregularities, two types of shapes could be distinguished within the irregularities. In one type, the largest probabilities were found at the lowest, or calm speeds, with an almost monotonic decay of probability with increasing speed. In the second type, which is bell-shaped, there was an almost zero probability at calm speeds, rising to a single or to multiple modes at moderately low speeds and then exhibiting rapid decay at larger speeds. From physical reasoning, this second type, with zero probability at calm speeds, would seem to be most logical. In fact, it might be suspected that the first type could to some extent indicate the high probability of calm speeds because of an instrument insensitivity threshold. Figure 3 shows examples at the Goldstone Mars site 46-m anemometer for these two types; the February 1968 data is representative of the monotonically decaying shape and the April 1968 data illustrates the bell shape.

Both of these curves are also characterized by irregularities in the form of spikes and sags. This appears to be typical of the wind speeds that have been observed at this and the other Mojave Desert reference sites. The corresponding wind speed distributions are shown on Fig. 4. These distributions are considerably smoother because of the integrating effect, which tends to remove the irregularities.

Figure 5 shows probability density curves for all of the Goldstone data at the 46-m anemometer for the year 1967 (2758 measurements) and the year 1968 (5395 measurements). The 1967 data tends to indicate the almost monotonically decaying shape, and the 1968 data tends to exhibit the bell-shaped type of function. These curves again display the aforementioned irregularities in shape. The distribution functions, shown on Fig. 6, are smooth, as expected. Although the two curves shown on Figs. 5 and 6 might not appear to differ excessively on cursory examination, their relative agreement could be deceiving with respect to the available wind power. Computations of the wind power for these two sets of data shows that the 1967 data indicated from 1.5 to 2.5 times as much available wind power, depending upon parameter choices for the wind power generator, as the power available for 1968. Because of the cube law of power variation with speed, visual interpretation of density or distribution functions could be deceiving with respect to available power. In Section III, a more appropriate statistical function for power prediction will be discussed.

The parameters of several theoretical functional forms of probability distributions were empirically fit to the data to determine which of these functions could provide reasonable representations. The most appropriate of these were found to be (a) Pearson Type III, (b) Gamma, (c) Weibull, and (d) a modified exponential. In the literature, the equations of these functions
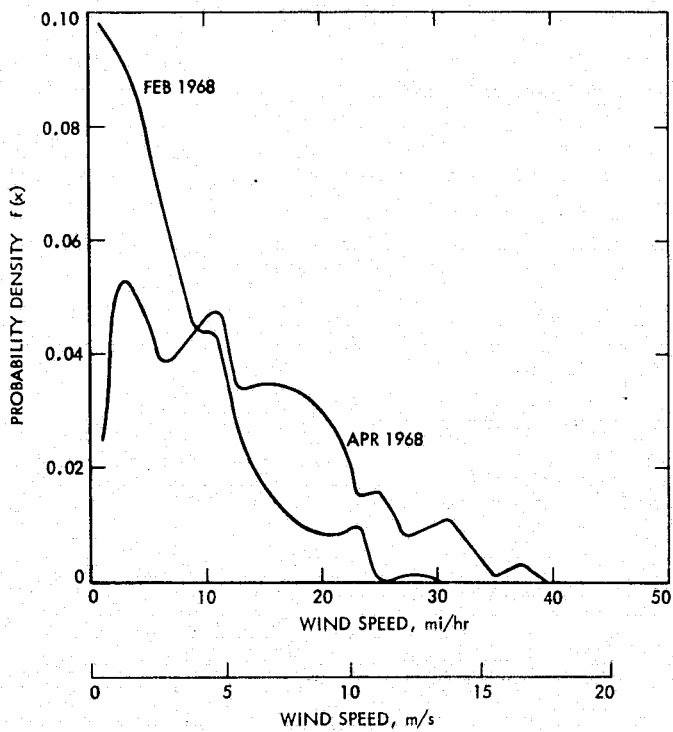
Fig. 3. Examples of empirical probability
density at Goldstone
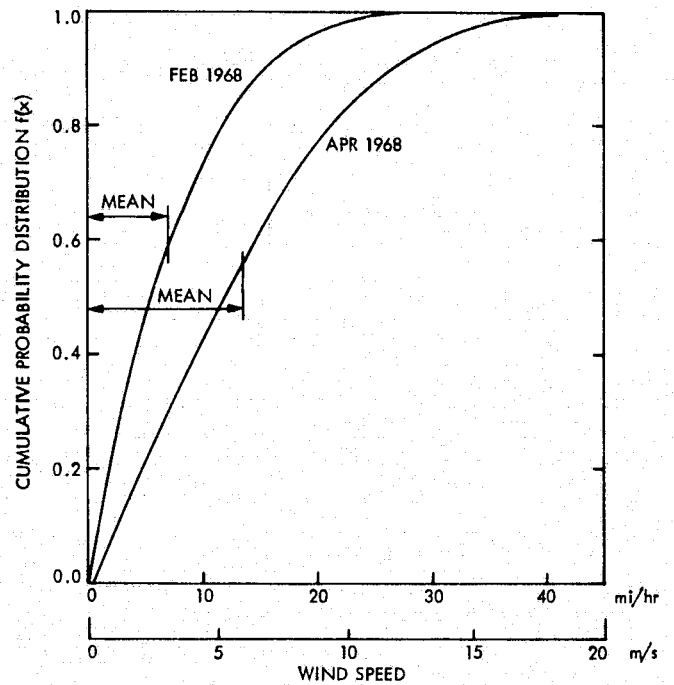
Fig. 4. Examples of probability distri-
bution at Goldstone
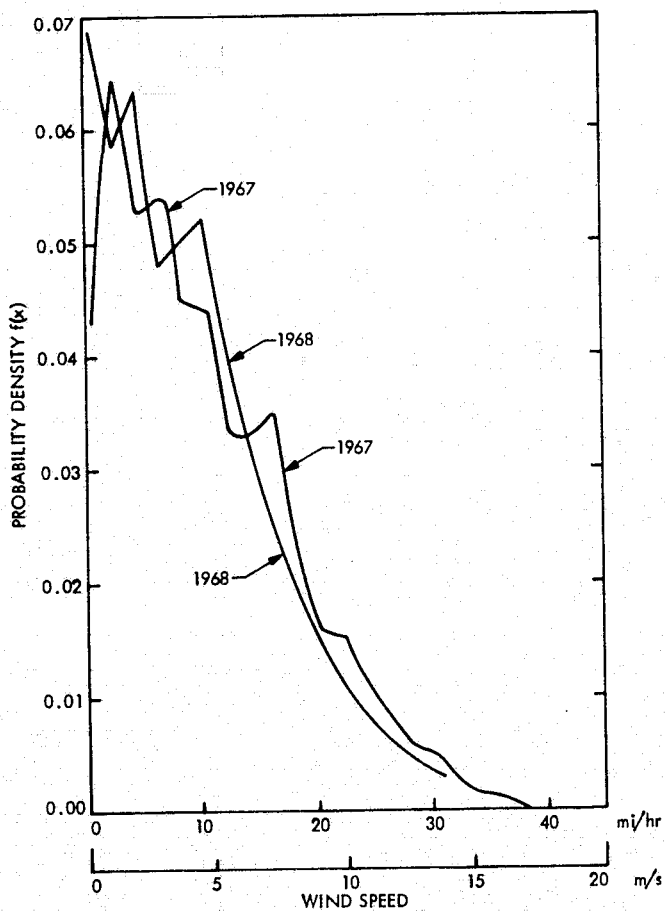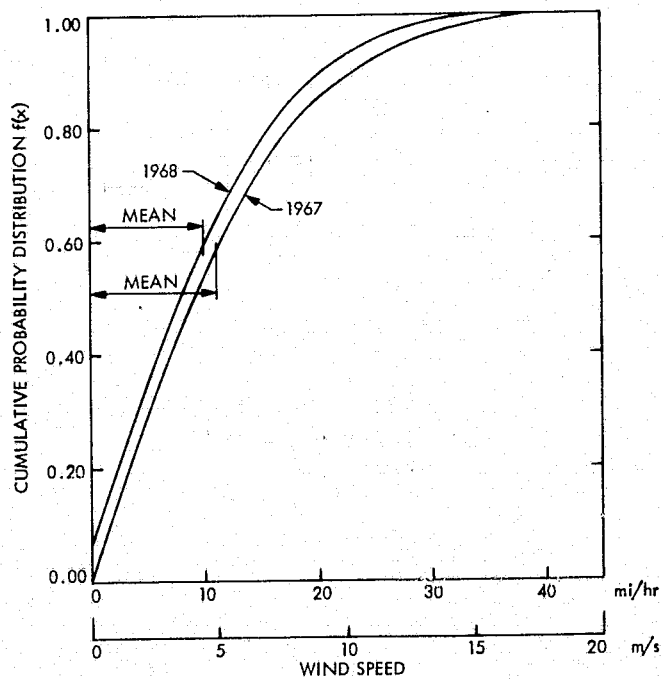
Fig. 5. Mars site annual probability densities

Fig. 6. Mars site annual probability distributions

appear in several alternative forms, so that for completeness we will give the forms used here. Typical notation and definitions are given in Table 4.

1. Pearson Type III

This is a 3-parameter function that can assume a variety of shapes, depending upon its parameters, and can also degenerate to other well-known probability functions. Because of the variety of shapes possible, it has been suggested (Ref. 1) as useful in modeling wind speeds. Theoretically, however, it has a minor defect in admitting the probability of a few small negative values of the speeds. The equations are most conveniently expressed in terms of a standardized variate t, and a parameter A. The variate t is standardized in terms of the wind speed x, and its standard deviation σ, by the equation

$$t = (X - m_1)/\sigma \tag{1}$$

and A is found from

$$A = 2/a_3 \tag{2}$$

where a_3 is the skewness and m_1 is the mean as defined in Table 4. The density function is

$$f(t) = A[A(A+t)]^{A^2-1} \exp[-A(A+t)]/\Gamma(A^2) \tag{3}$$

where $\Gamma(.)$ is the gamma function. The wind speed density can be recovered from the density of t by

$$f(x) = f(t)/\sigma \tag{4}$$

Note that Eq. (3) indicates only a single parameter A, but incorporates in t the remaining two parameters of mean and standard deviation. By a transformation of variables, the Pearson III density can be transformed (Ref. 2) into the chi-square distribution, which is more readily available in tabulations and subroutines. To make the transformation, using y as the chi-square variate and v as the chi-square parameter, let

$$y = 2A(A+t) \tag{5}$$

$$v = 2A^2 \tag{6}$$

Then

$$f(t) = \sqrt{2V} \; f(y) \tag{7}$$

and the distributions of t and the chi-square variate are the same. That is,

$$F(t) = F(y) \tag{8}$$

Table 4. Notations and definitions

Definition	Sample computational form (N = number of terms)
Moments about the origin	
m_1 = first moment (mean)	$\Sigma X_i/N$
m_2 = second moment	$\Sigma X_i^2/N$
m_3 = third moment	$\Sigma X_i^3/N$
Central moments	
U_2 = second (variance)	$m_2 - m_1^2$
U_3 = third	$m_3 - 3m_2m_1 + 2m_1^3$
Additional definitions	
σ = standard deviation	$\sqrt{U_2}$
V = coefficient of variation	σ/m_1
a_3 = skewness	U_3/σ^3
$E[.]$ = expectation	$E[X^k] = m_k; \quad E[(X - m_1)^k] = U_k$
$f(x)$ = probability density function	
$F(x)$ = cumulative distribution function	

2.   Gamma Distribution

This distribution applies for a positive random variable and has parameters that depend upon the mean and standard deviation only. It can be shown that by a change of variables the gamma distribution is a special case of Pearson III. The parameters are a scale factor λ and a shape factor G, where

$$\lambda = m_1/\sigma^2 \tag{9}$$

$$G = m_1\lambda = m_1^2/\sigma^2 \tag{10}$$

The density function is

$$f(x) = \lambda(\lambda x)^{G-1} \exp(-\lambda x)/\Gamma(G) \tag{11}$$

The distribution function, which requires the incomplete gamma function, is

$$F(x) = \Gamma(G,\lambda x)/\Gamma(G) \tag{12}$$

When G has the value of unity, the gamma distribution degenerates to the exponential, and when G is greater, the distribution is bell-shaped and skewed. Thus the gamma distribution has the capability of producing the observed shapes of wind speed density data.

3.   Weibull Distribution

This was proposed by Weibull (Ref. 3) to have a theoretical justification in the weakest link type of failure, as for a chain. Consequently, its use is widespread in reliability analysis. He also proposed this distribution as capable of fitting many types of observations regardless of the theoretical basis. As in the case of the gamma distribution, it applies only to random variables. Davenport (Ref. 4) recommended this distribution to model wind speeds with both physical and experimental justification. The density function is defined in terms of a shape parameter K and a scale factor C so that

$$f(x) = K/C(x/C)^{K-1} \exp -(x/C)^K \tag{13}$$

The parameters can be found indirectly from the mean and standard deviation as follows

$$1 + (\sigma/m_1)^2 = [\Gamma(1 + 2/K)]/[\Gamma^2(1 + 1/K)] \tag{14}$$

A numerical solution can be performed to find K to satisfy Eq. (14). Then C can be found from

$$C = m_1/\Gamma(1 + 1/K) \tag{15}$$

The distribution function is

$$F(x) = 1 -\exp[-(x/C)^K] \tag{16}$$

4.   Modified Exponential Distribution

The standard exponential distribution is defined for positive random variables in terms of a single parameter B. The density function is

$$f(x) = B \exp(- Bx) \qquad (17)$$

The parameter B is equal to the mean, which is also the standard deviation. The shape of the density decays exponentially from a peak at the origin. This shape is too limited to represent the observed wind densities. A modified 2-parameter form of the equation was proposed to permit both the skewed bell-shape as well as the exponential shape. The modified form has the following density function with parameters a,b

$$f(x) = (a + 2bx) \exp [-(ax + bx^2)] \qquad (18)$$

The distribution function is

$$F(x) = 1 -\exp [-(ax + bx^2)] \qquad (19)$$

This distribution was used primarily for the work on the interim simulation model, which will be discussed subsequently, as will the method used to determine the two parameters.

C.   COMPARISON OF FITTING FUNCTIONS

Numerous sets of the four foregoing types of functions have been fit to the Goldstone data and also the data for the supplementary Mojave Desert airport sites. Comparisons of the closeness of the fits show that the Pearson III, Weibull, and modified exponential all tend to be reasonable and about equivalent. The gamma function sometimes provides a less accurate fit than the other three. In all cases, because of the irregularities in the empirical density functions (see Figs. 3 and 5), noticeable differences appear when these functions are plotted against the empirical functions. However, when the plots of the cumulative distributions are compared, the differences from the empirical tend to be extremely small and often indistinguishable.

Figure 7 contains a repetition of the February 1968 empirical density for comparison with curves of the fitting Weibull and modified exponential functions. Both of these appear to approximate the empirical very well. Figure 8 repeats the April 1968 data for comparison with the Pearson III and gamma fitting functions. Neither of these two forms (nor the modified exponential and Weibull as well) have the capability of matching the double mode in the empirical data that appears at low wind speeds. The Pearson III curve tends to fair itself in near the top of the double mode peaks, while the gamma function tends to overshoot the peaks. The Weibull and modified exponential, which for clarity are not plotted here, would both be somewhat lower than the Pearson III and gamma curves at the peaks, and all four types of curves fair in to the empirical curve about equivalently at the higher wind speeds.

Because all four types of fitting functions closely approximate the empirical distribution functions, it is difficult to make graphical comparisons because large sections of the curves would coincide. As an alternative,
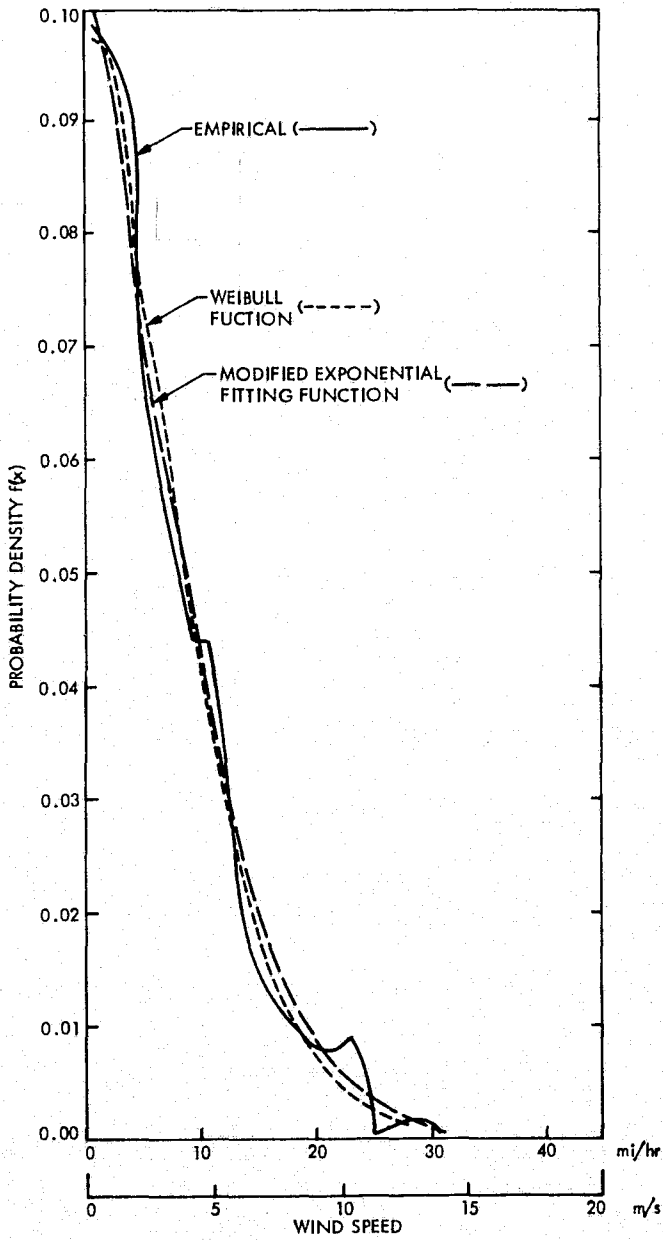
Fig. 7. Example of functions fit to February 1968 empirical probability density
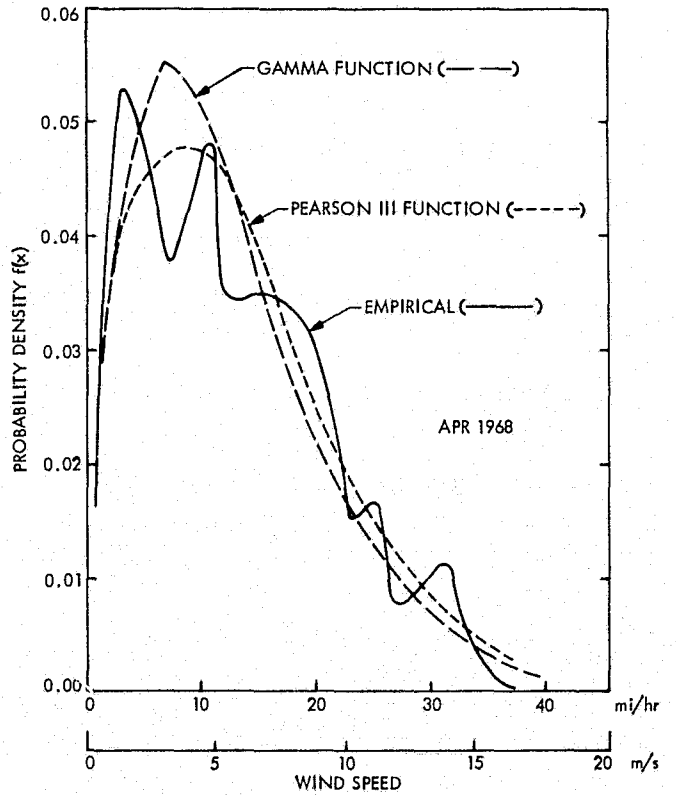
Fig. 8. Example of functions fit to April 1968 empirical probability density

Tables 5 and 6 contain tabulations of the empirical and fitting function distributions from February and April 1968 for comparison. From Table 5 it can be found that the maximum differences between distributions of the fitting functions and the empirical are 0.026, 0.029, 0.014, and 0.013 for the Pearson III, gamma, Weibull, and modified exponential. From Table 6, the corresponding maximum differences are 0.018, 0.038, 0.022, and 0.014.

If it is necessary to select one of the four fitting functions for general application to wind speed densities and distributions, the Weibull function is recommended. Although the Pearson III, Weibull, and modified exponential functions appear to perform equivalently, the Pearson III is less preferable since it requires three rather than two parameters for its definition. Since the Weibull is a well-known function that is familiar within the literature, it would seem to be preferable to the modified exponential for retention. The latter was an ad hoc suggestion that was found to work well for the present program, but is not in general use.

Table 5. February 1968 wind speed distributions

Wind speed, m/s	mi/hr	Empirical[a]	Fitting function			
			Pearson III	Gamma	Weibull	Modified exponential
0.4	1.0	0.099	0.115	0.070	0.064	0.106
1.3	3.0	0.293	0.273	0.274	0.283	0.297
2.2	5.0	0.465	0.439	0.463	0.462	0.460
3.1	7.0	0.601	0.586	0.613	0.606	0.594
4.0	9.0	0.704	0.705	0.725	0.718	0.702
4.9	11.0	0.792	0.795	0.807	0.801	0.785
5.8	13.0	0.862	0.861	0.866	0.862	0.849
6.7	15.0	0.904	0.907	0.908	0.905	0.896
7.6	17.0	0.929	0.939	0.935	0.936	0.930
8.5	19.0	0.948	0.960	0.956	0.956	0.954
9.4	21.0	0.965	0.974	0.970	0.971	0.970
10.3	23.0	0.932	0.983	0.980	0.981	0.981
11.2	25.0	0.991	0.989	0.986	0.988	0.988
12.1	27.0	0.993	0.993	0.991	0.992	0.993

[a]Data at Goldstone MARS tower 46-m anemometer.

Table 6. April 1968 wind speed distributions

Wind speed, m/s	mi/hr	Empirical[a]	Fitting function			
			Pearson III	Gamma	Weibull	Modified exponential
0.4	1.0	0.025	0.042	0.008	0.018	0.032
1.3	3.0	0.102	0.098	0.067	0.090	0.106
2.2	5.0	0.203	0.178	0.162	0.182	0.189
3.1	7.0	0.290	0.267	0.271	0.281	0.277
4.0	9.0	0.372	0.364	0.381	0.380	0.367
4.9	11.0	0.464	0.461	0.483	0.475	0.456
5.8	13.0	0.547	0.552	0.575	0.562	0.541
6.7	15.0	0.617	0.633	0.655	0.639	0.619
7.6	17.0	0.687	0.705	0.722	0.707	0.690
8.5	19.0	0.755	0.765	0.778	0.765	0.752
9.4	21.0	0.815	0.816	0.824	0.814	0.805
10.3	23.0	0.856	0.857	0.861	0.854	0.852
11.2	25.0	0.889	0.890	0.892	0.886	0.886
12.1	27.0	0.914	0.916	0.915	0.913	0.915
13.0	29.0	0.931	0.937	0.934	0.933	0.938
13.9	31.0	0.953	0.952	0.949	0.950	0.956
14.8	33.0	0.970	0.964	0.961	0.963	0.969
15.6	35.0	0.978	0.973	0.969	0.972	0.978
16.5	37.0	0.983	0.981	0.976	0.979	0.985
17.4	39.0	0.987	0.986	0.982	0.985	0.990
18.3	41.0	0.990	0.989	0.986	0.989	0.994
19.2	43.0	0.993	0.992	0.989	0.992	0.996

[a]Data at Goldstone MARS tower 46-m anemometer.

III. WIND POWER PREDICTION MODEL

A. POWER PREDICTION EQUATION

The kinetic energy of the wind passing through a unit area in a unit time is the instantaneous power per unit area incident on the collector. If the air has mass density ρ and wind speed x, the power on the unit area is

$$P_A = 1/2\,\rho\,x^3 \tag{20}$$

In Eq. (20), P_A will be in watts per square meter when ρ is in kilograms per cubic meter and x is in meters per second. Since wind speeds are frequently measured and tabulated in miles per hour, these can be converted to meters per second by multiplying by 0.447.

When the wind speed varies during a given time period, the average power during this period can be computed in terms of the expected (average) value of the cube of the speed, $E[x^3]$, or

$$P_A = 1/2\,\rho\,E[x^3] \tag{21}$$

If the speed is assumed to be a continuous random variable, the expectation can be expressed (Ref. 5) in terms of the probability density function of the speed as

$$E[x^3] = \int x^3\,f(x)\,dx \tag{22}$$

where the limits of integration extend over all realizable values of x, or in this case from zero to x_m, the maximum value. Consequently, the average power per unit area can be stated as

$$P_A = (1/2)\rho \int_0^{x_m} x^3\,f(x)\,dx \tag{23}$$

The integral in Eq. (23) can be replaced by a "pattern factor" (Ref. 6) K_e, which in terms of the notation used here is equivalent to

$$K_e = \frac{1}{m^3} \int_0^{x_m} x^3\,f(x)\,dx \tag{24}$$

in which $m = m_1$ (see Table 4) is the average wind speed. Consequently, Eq. (23) becomes

$$P_A = 1/2\,\rho\,K_e\,m^3 \tag{25}$$

For application to power prediction at candidate windmill sites, it is necessary to recognize that practical windmills do not operate to use all the power available in the highest wind speeds. At high wind speeds, the generators either shut down to produce no power at speeds exceeding a cutoff speed x_c, or the operation is throttled or feathered to continue operating

but to generate no more power than would be available at the cutoff speed. Consequently, instead of using K_e in Eq. (25), either of two new modified pattern factor terms S_3 or S_{3F} can be used to represent the shutdown or throttled cases, respectively, where

$$S_3 = \frac{1}{m^3} \int_0^{x_c} x^3 \, f(x) \, dx \qquad (26)$$

and

$$S_{3F} = \frac{1}{m^3} \int_0^{x_m} \min \, (x^3, x_c^3) dx \qquad (27)$$

It can be seen that in Eqs. (26) and (27), S_3 and S_{3F} are functions of x_c. By introducing a factor β, where

$$\beta = X_c/m \qquad (28)$$

so that

$$X_c = \beta m \qquad (29)$$

both S_3 and S_{3F} become functions of β. It will be shown subsequently that these two functions when defined as above, and for the practical values of β, exhibit only relatively small variations when they are computed for the annual records of observed data at Goldstone and the supplementary Mojave Desert airport sites. Using either of these two factors, the average power is then given by

$$P_A = 1/2 \, \rho \, S_3(\beta) m^3 \qquad (30a)$$

or

$$P_A = 1/2 \, \rho \, S_{3F}(\beta) m^3 \qquad (30b)$$

Consequently, Eqs. (30a) and (30b) are the equations for estimating the average power at a site. The subsequent discussions will cover methods of estimating the three necessary terms (ρ, S_3 and m) for applying the equations to Goldstone windmill sites.

B.   FACTORS OF THE POWER PREDICTION EQUATION

1.   Air Density

Variations in this factor are primarily the result of the random air temperature. Other physical constants upon which the density depends will be considered as essentially deterministic. In particular, observed variations at Goldstone of barometric pressure at constant temperature would have only a secondary effect.

The density will be obtained by first expressing density as a deterministic function of the atmosphere pressure and then relating pressure to the random effect of temperature. To do this in international system units let

p = the pressure at any altitude

p_a = the pressure at sea level for standard conditions, 101,000 N/m^2

T_k = temperature at any altitude, K

T_a = absolute temperature at sea level, 290°K

β = temperate gradient with elevation, 0.0065°K/m

R = gas constant, 287 m^2/s^2°K

g = acceleration of gravity, 9.8 m/s^2

c = g/Rβ = 5.256

ρ = density, kg/m^3

z = altitude above sea level, average 1070 m at Goldstone

The density is related to the pressure by the gas law equation

$$\rho = p/(RT) \qquad (31)$$

Pressure is related to temperature through the following equation

$$(p/p_a) = \left[1 - \beta z/T_a\right]^c \qquad (32)$$

Substituting the tabulated constants into Eq. (32), we obtain

$$p = 101000 \; [1-(0.0065)(1070)/288]^{5.256}$$

$$= 88,900 \text{ N/m}^2$$

Solving for ρ from Eq. (31), we have

$$\rho = 88,900/(287T_k) = 308/T_k \text{ kg/m}^3$$

An estimate of T_k was obtained from a record of the Goldstone temperatures during the year 1972. This record contained daily minimum and maximum temperatures, which were averaged as an estimate of the daily average temperature. Twelve monthly pools of these daily averages were assembled, which gave the following 12-component vector of monthly average temperatures (°F) (45, 52, 63, 60, 68, 78, 85, 82, 70, 60, 48, 45). The average of this vector is 63°F = 523°R. The sample standard deviation is 14.0°F. In Kelvin temperature units the average absolute temperature is 290 and the standard deviation is 7.8. Therefore, the average density of the air at Goldstone (kg/m^3) is

$$\rho = 308/290 = 1.0621$$

The variance depends upon the variance of the air temperature and is approximately

$$VAR\, \rho \cong VAR\, T_k (308/T_k^2)^2$$

The standard deviation and coefficient of variation then become, respectively

$$\sigma(\rho) = (VAR\, \rho)^{1/2} = (7.8)(308)/(290)^2 = 0.029$$

and

$$V(\rho) = 0.029/1.0621 = 0.027$$

2.   Modified Pattern Factors

The modified pattern factors will be presented here in two forms. The first form will be denoted as S_3 for the case of shutdown at the cutoff speed x_c; the second will be denoted as S_{3F} for the case of continued operation at the cutoff speed for winds that exceed the cutoff speed.

To cover a spectrum of alternative cutoff speeds, it is necessary to describe S_3 or S_{3F} by a vector with individual components that correspond to specific cutoff speeds. The cutoff speeds normalized by the average speed will be described by a parameter β defined by

$$\beta = x_c/m \qquad (33)$$

where x_c is the cutoff speed and m is the average speed.

For the present, values of the statistics are to be considered as those that would be obtained on an annual basis. If these are applied to the prediction of the power for a shorter period, say monthly or weekly, the appropriate statistics will have greater variability than will be indicated here.

A data base consisting of weather bureau statistics for a total of 36 years at the three supplementary Mojave Desert airport sites (Table 2) was used to determine the statistics of S_3 and S_{3F}. The data from each year of records was averaged over the year to determine S_3 or S_{3F} as annual average statistics. Then all of the annual statistics were pooled to determine the composite average. The statistics were determined at increments of $\beta = 0.25$, beginning at $\beta = 1.0$ and ending at $\beta = 4.5$. A summary of the composite resulting statistics for sample averages, standard deviations and coefficients of variation for values of β to 3.5 is given in Table 7. For practical windmill design, the range of β might be from 1.5 to 3.0. Within this range, the small coefficients of variation, which are generally less than 10%, indicate the relatively small uncertainty in the average pattern factors. The pattern factors are plotted in Fig. 9.

A breakdown of the averages for each of the sources that were used in the 36-year composite averages is shown in Table 8. In addition, the averages for Goldstone for two partial years of data at the 46-m (150-ft) anemometer are also shown for comparison. These Goldstone averages are plotted on Fig. 10. The close correspondence between the two Goldstone cases and the 36-year composite results in some cases makes it impossible to distinguish

Table 7. 36-year composite averages of modified pattern factors

Station period	S_3			S_{3F}		
	Average	Standard deviation	Coefficient of variation	Average	Standard deviation	Coefficient of variation
1.0	0.173	0.054	0.34	0.585	0.041	0.070
1.25	0.352	0.088	0.250	0.936	0.030	0.033
1.50	0.574	0.084	0.146	1.319	0.053	0.040
1.75	0.879	0.089	0.101	1.714	0.115	0.067
2.00	1.275	0.111	0.087	2.075	0.196	0.095
2.25	1.673	0.103	0.062	2.365	0.291	0.123
2.50	2.054	0.171	0.083	2.579	0.380	0.147
2.75	2.373	0.290	0.122	2.726	0.455	0.167
3.00	2.581	0.385	0.149	2.814	0.504	0.179
3.25	2.710	0.448	0.166	2.867	0.535	0.187
3.50	2.809	0.500	0.178	2.898	0.555	0.192

Table 8. Pattern factor averages from individual sources

| Station period | S_3 averages | | | | | |
	George, 51-55	Edwards, 50-54	Edwards, 57-70	Daggett, 62-73	Goldstone, 67	68
β						
1.0	0.229	0.125	0.130	0.221	0.151	0.154
1.25	0.417	0.292	0.272	0.454	0.315	0.338
1.50	0.584	0.530	0.499	0.674	0.565	0.585
1.75	0.867	0.859	0.817	0.965	0.829	0.877
2.0	1.167	1.382	1.217	1.344	1.197	1.215
2.25	1.528	1.715	1.692	1.695	1.509	1.541
2.50	1.879	2.268	2.162	1.917	1.854	1.881
2.75	2.145	2.685	2.606	2.065	2.240	2.218
3.00	2.365	2.914	2.910	2.150	2.482	2.462
3.25	2.535	3.041	3.092	2.198	2.639	2.726
3.50	2.652	3.174	3.213	2.250	2.711	2.881
	S_{3F} averages					
1.0	0.596	0.570	0.546	0.633	0.544	0.557
1.25	0.909	0.951	0.915	0.964	0.887	0.911
1.50	1.241	1.394	1.343	1.293	1.267	1.292
1.75	1.596	1.862	1.796	1.607	1.640	1.671
2.0	1.920	2.285	2.229	1.871	1.995	2.025
2.25	2.200	2.623	2.606	2.045	2.295	2.339
2.50	2.419	2.877	2.899	2.149	2.551	2.605
2.75	2.575	3.051	3.106	2.211	2.740	2.819
3.00	2.684	3.142	3.230	2.246	2.868	2.979
3.25	2.758	3.195	3.302	2.268	2.961	3.103
3.50	2.804	3.225	3.345	2.280	3.038	3.187

STATION	GEORGE	EDWARDS	EDWARDS	DAGGETT
YEARS	1951–55	1950–54	1957–70	1962–73
N	5	5	14	12
ANEMOMETER HT, m (ft)	24 (80)	9.75 (32)	4 (13)	6 (20)
AVG SPEED m/s (mi/hr)	4.45 (9.97)	4.32 (9.68)	3.76 (8.41)	5 (11.15)
STD DEV, m/s (mi/hr)	0.47 (1.05)	0.5 (1.12)	0.3 (0.65)	0.3 (0.71)

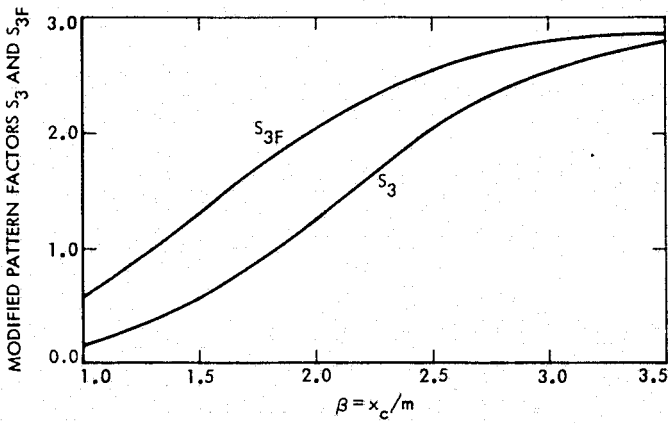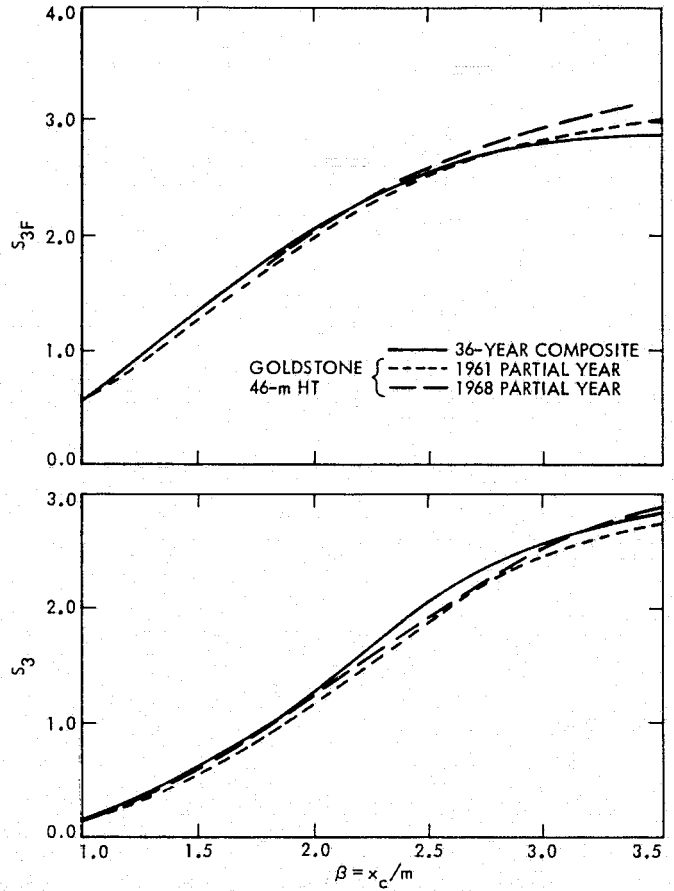Fig. 9. 36-year composite pattern factors

Fig. 10. Pattern factors for two years at Goldstone

the plots. This is again further evidence that these average pattern factors are stable for estimating the average available wind power at these sites.

The cumulative probability density functions for the sets of 36 points used to compute $S_3(2.0)$ and $S_3(2.5)$ are shown on Figs. 11 and 12. The ordinate scale is drawn to percentage points of the normal distribution. The abscissa scale is logarithmic (linear in $\ln S_3$). The straight lines approximating the points were determined for the assumption of a logarithmic normal distribution. From the proximity of the points to the lines, the lognormal distribution tentatively seems reasonable to approximate S_3. Nevertheless these figures show points that are displaced by as much as 6% (distribution scale) with respect to the approximating lines.

Examination of Fig. 9 shows that at the higher values of β the S_3 and S_{3F} curves tend to converge. As expected, these curves approach each other when the cutoff speed is equal to the maximum speed for the period of record. At this speed there is no more power to be gained by increasing β. Examination of single-year compilations of S_3 from the many individual cases shows the maximum wind speed in a year rarely gets as high as 4 times the average. In some years the maximum is no more than about 2 times the average. Multiyear data pools have been assembled to determine the empirical cumulative frequency distributions for the sets of data groups that have been considered in this section. These are plotted on Fig. 13. It can be deduced for example, that if x_c is set at 20 mph (β between 2.0 and 2.5 for most of this data), the system will be operating below full capacity about 90% of the time. Consequently, it is not likely that practical windmills will be designed for the relatively larger values of β, so that in the expected design range of relatively low values of β, the tabulated values of the modified pattern factors S_3 tend to have relatively small dispersion.

3. Average Wind Speeds

The average wind speed as required for the application of the power prediction equation, Eq. (30), is the most uncertain factor in the equation. When a substantial amount of data is available for a particular site, much of the uncertainty tends to be overcome. However, for new proposed sites there is less likely to be a significant amount of data. In these cases, it is reasonable to use whatever data is available for the new site and to try to extend this information by correlation with similar sites for which more data is available.

Recorded wind speed data usually represents the hourly average wind speeds. This type of recording tends to wash out the small time-scale turbulent variations in the wind speeds. Wind turbulence, if recorded, would indicate additional power available from the wind beyond the power calculated from the average speed. Whether or not the windmill can respond to use the additional power depends on the dynamics of the windmill structure and its control system. However, it is useful to be able to estimate the additional power beyond that contained in the mean wind speed. When the system is designed, it then may be possible to decide how much of this can be exploited.

Frequently the information that is available to estimate the mean speed at a proposed site is derived from anemometer heights that do not coincide with the height above ground for the proposed windmill. Consequently, it is
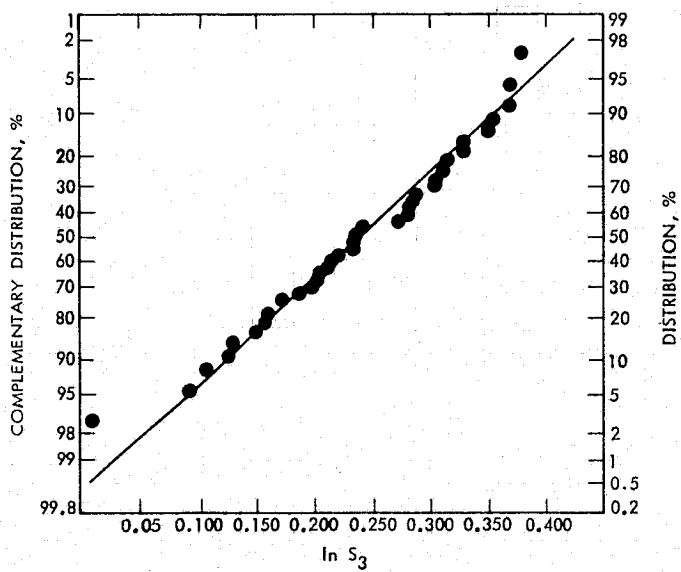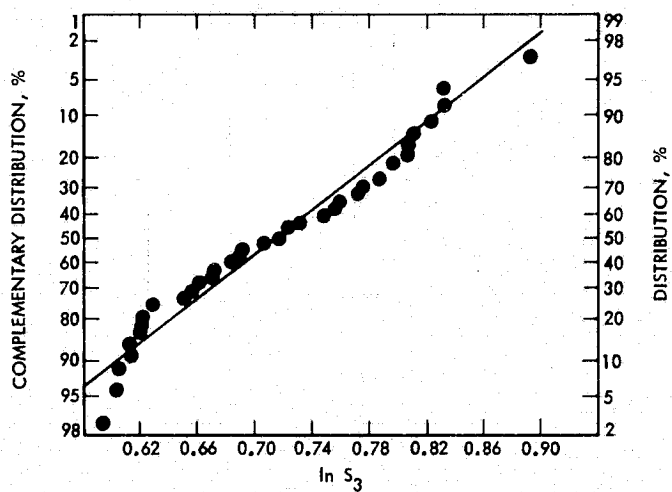
Fig. 11. Distribution of S_3 (2.0)

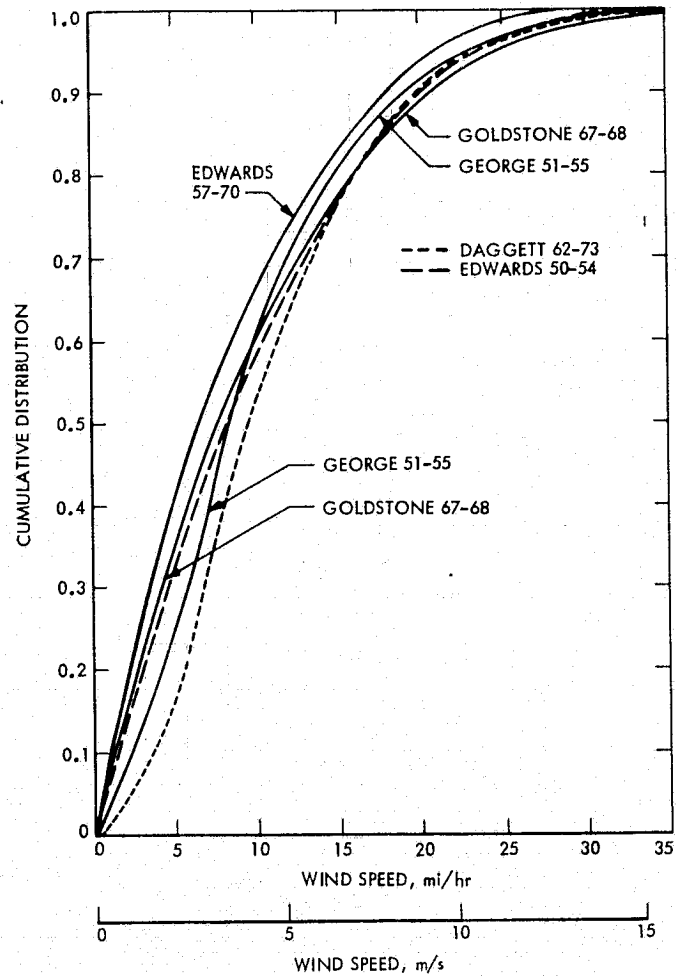Fig. 12. Distribution of S_3 (2.5)

Fig. 13. Wind speed distribution for multiple-year data pools

useful to have a scaling law to predict the profile of wind speed variation with height above ground. Well-known formulations are available to derive mean speed vs ground height variations.

a. <u>Wind Profile</u>. The relationship conventionally adopted in civil engineering practice to describe the variation of wind speed with the height profile is

$$V_A/V_0 = (z_A/z_0)^\alpha \qquad (34)$$

where

V_A is the wind speed at height z_A

V_0 is the wind speed at a reference height z_0

α is the power law exponent, typically considered to have the approximate range of 1/7 (flat open country) to 1/2.5 (urban areas)

Equation (1) is considered to be applicable in the neighborhood of a smooth boundary with moderate values of the Reynolds number (Ref. 7). A more general logarithmic speed profile law is given in the form (Refs. 7,8)

$$V_A = 2.5U^*\ln(z_A - z_d)/z_0 \qquad (35)$$

where U^*, z_d, z_0 are parameters that vary with the terrain.

Because of the computational advantage of having a single unknown parameter (but with well-known typical ranges) and the scatter that has been observed in the data that is available, Eq. (34) will be adopted here in preference to the more complex Eq. (35). Preliminary examinations of application of Eq. (35), including parameter fitting to available Goldstone data, indicate that the three necessary parameters tend individually to exhibit wide variations in magnitude from site to site, although when combined they produce a stable speed profile. In any case, either of these two equations produces equivalent results when applied to the Goldstone data.

Data pools of monthly average speed determined at Goldstone at the 15-m (50-ft), 46-m (150-ft) and 91-m (300-ft) vector vane anemometer heights of the Mars site tower are given in Table 9. These 22 pairs of data were used to perform a regression analysis to determine the least squares value of the parameter α, using the 15-m-high anemometer as the reference. A linear equation for the regression analysis is obtained by taking the logarithms of both sides of Eq. (34); e.g.,

$$\text{Log } V_A/V_0 = \text{Log } z_A/z_0 \qquad (36)$$

The value of α was found to be 0.1405, which is close to the value (1/7) to be expected for the local terrain. However, it should be noted that the standard deviation of this estimated value of α was 0.0193, which permits a substantial amount of dispersion when speed ratios are computed according to Eq. (34). Plotting the 22 speed ratios that can be determined from Table 9 against the speed ratio curve predicted from Eq. (34) would show considerable scatter with respect to the curve. There would be no reduction in the scatter

Table 9. Monthly average wind speeds at Mars site at heights

of 15-46-91 m (50-150-300 ft)

V_i = average speed for month, mph

n_i = number of observations in the month

| Year | Month | 15 m (50 ft) | | 46 m (150 ft) | | 91 m (300 ft) | |
		V_i	n_i	V_i	n_i	V_i	n_i
1966	9	8.210[a]	607	7.388[a]	603	10.825[a]	490
	10	6.947[a]	716	7.440[a]	695	9.807[a]	703
	11	6.442	704	8.834	703	9.280	756
	12	8.347	245	11.014	246		
1967	1	8.442	210	13.167	245		
	2	8.012	210	10.709	110	9.117	149
	3	12.893	207	14.638	244	15.347	243
	4	12.674	237	15.498	238	15.990	239
	5	11.150	242	12.774	243	12.798	239
	6	10.532	225	11.072	117	12.190	229
	7	9.696	197	10.778	197	10.794	188
	8	7.240	247	8.240	246	8.497	244

[a]Averages computed from tabulations of frequency of occurrence at 5-mph class intervals. For other entries, average computed directly from n_i terms as given on punched card records.

if the logarithmic profile were to be used. This follows because when Eq.
(35) is used to fit a curve passing through the regression predictions at
the 15-, 46-, and 91-m heights, the two curves are indistinguishable. Conse-
quently, there is little practical difference in the choice of either power
law or logarithmic profile law.

    b.   <u>Wind Turbulence</u>. Data bases typically consist of wind speeds
averaged over relatively long periods of time. Therefore, the data is a
smoothed average from which the short-term local variations (turbulence)
have been filtered. As will be shown, there is actually more power available
to a wind turbine than the averaged data indicates.

    A convenient model for the total wind V_t that includes the turbulences
is to consider this as the sum of a quasi-steady component m and a turbulent
gust component v. That is,

$$V_t = m + v \qquad\qquad (37)$$

The quasi-steady component actually has time variations for which spectral
decompositions would show predominant periods in the order of days. The
turbulent component spectrum shows predominant periods in the order of minutes
to seconds. A spectral gap centered at periods of about one hour separates
the two components (Ref. 9).

    The total power available from the wind (Eq. 20) is a function of the
cube of the total speed, or cubing the right-hand side of Eq. (37) and taking
expectations gives the expected value of the cube of the total wind speed,
or

$$E[V_t^3] = E[(m + v)^3] \qquad\qquad (38)$$

where the symbol E [.] is used to denote expectation. Expanding the right-
hand side of Eq. (38), normalizing by m^3, and treating m as a constant results
in

$$E[V_t^3/m^3] = 1 + 3E[v^2]/m^2 + 3E[v]/m + E[v^3]/m^3 \qquad\qquad (39)$$

If we make the usual assumption that the turbulent component has mean zero,
the expectations of all odd powers disappear. Then Eq. (39) can be simplified
to

$$E[V_t^3/m^3] = 1 + 3a$$

where

$$a = E[v^2]/m^2 \qquad\qquad (40)$$

Note that the new term "a" is equivalent to the ratio of the mean square
of the turbulent component to the mean square of the steady component.

    The mean square of the turbulent component is related to the mean square
of the steady component by the empirical equation

$$E[v^2] = 6K\,U_1^2 \qquad\qquad (41)$$

where K is the surface drag coefficient and U_1^2 is the steady speed at a height of 10 meters above ground. At any other height z_A with steady speed m we can apply the power law variation relationship to obtain

$$U_1 = (10/z_A)^\alpha m \tag{42}$$

Therefore, using Eqs. (42) and (41) provides

$$a = 6K (10/z_A)^{2\alpha} \tag{43}$$

To estimate K, the following values are typically stated:

Exposure	K
Flat, open country	0.005
Wooded country, coastal area, suburban area	0.010
Urban area	0.025

Estimating the value of K as 0.005 for Goldstone we have for an average value of a

$$a = 0.030 (10/z_A)^{2\alpha} \tag{44}$$

For example, with $\alpha = 0.1405$, $z_A = 46$ m, we have

$$a = 0.030 (10/46)^{0.2810} = 0.0195$$

Consequently, for use in Eq. (30), the mean speed could be adjusted by a factor of

$$[1 + 3(0.0195)]^{1/3} = 1.02$$

Cubing this factor shows that in this case the turbulence could increase the power by about 6%, depending upon the transfer function of the windmill system as related to the spectral decomposition of the turbulence.

One of the simplest and most widely known models for turbulence spectra is the Davenport (Ref. 10) model, giving the spectrum in the form

$$S(n) = (4/n)(K U_1^2) X^2/(1+X^2)^{4/3} \tag{45}$$

in which

$X = Ln/U_1$, where L is a scaled factor taken to be 1200 m

n = cycles/second

and K and U_1 are as already defined.

Note that Eq. (45) represents the spectrum as independent of the height above ground. Hino (Ref. 11) proposed an alternative expression that includes the effect above ground height z_A. His equation can be shown to be equivalent to

$$S(n) = (2.851/n)(KU_1{}^2)\ X_1/(1+X_1{}^2)^{5/6} \tag{46}$$

in which

$$X_1 = L_1 n/U_1$$

and

$$L_1 = 534.6\ (K^{1/2}/\alpha)^{3/2} \times 10(z_A/10)^{1-4\alpha}$$

Normalized spectra from Eqs. (45) and (46) for the three anemometer heights at the Mars tower are plotted on Fig. 14. This figure indicates the relatively low frequency in the wind gust spectra compared to frequencies of windmill structures, which would be expected to exceed several hertz. For example, at 46 m the spectrum in the figure peaks at about 0.0009 cycles/m. Taking U_i to be about 4 m/s, which is about the expected average speed at this site, we have

$$n = 4 \times 0.0009 = 0.0036\ \text{Hz}$$

At 100 times this frequency, which is still lower than the smallest structural resonance that might be expected, the spectrum has decayed to less than 10% of its peak. This indicates that the structure would respond to wind gusts as it would to a static load without either resonant amplification or attenuation. This would make the turbulence in the wind available for conversion to power within the capability of the control system dynamics. In the case of the example calculation, this would add about 6% to the total power.

c. Average Speeds at the Mars Site. The data base for the Mars site consists of the data observed during the 1966-68 period that is summarized in Table 1. This base in itself is much too brief to permit reasonable predictions for long-term annual speeds, since it consists of less than three years of incomplete records. On the other hand, relatively long annual records were available for the supplementary sites (Table 2). In particular, the Edwards and Daggett sites contained periods of time that were contemporary with the recording period at the Mars site. Consequently, it was reasonable to extend the Mars information by performing comparative analysis with Edwards and Daggett records in an attempt to extract a relationship between the wind speeds at these sites. Once found, the relationship could be used to extrapolate long-term speeds at the Mars site in terms of the known long-term speeds at the other two sites.

Two approaches were used to determine the relationship of wind speeds at the Mars site to the speeds at Edwards and Daggett. The first approach was a conventional regression analysis to determine a linear equation for the Mars speeds in terms of the other two. The second approach was a correlation analysis using the average speed observed at the Mars site and a correction
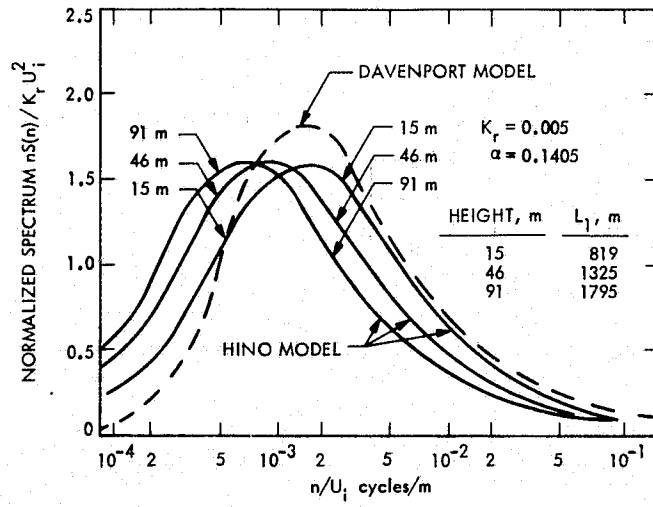
34

Fig. 14.   Mars site gust spectrum

term to account for long-term variations as deduced from the contemporary Edwards data and its deviation from the data observed at Edwards over 14 years (anemometer height 4.0 m = 13 ft).

(1) Regression Analysis. The regression equation is in the form

$$x_1 = b_{12} \, x_2 + b_{13} \, x_3 \tag{47}$$

where

x_1 is the predicted speed at Goldstone

x_2 is the speed at Edwards

x_3 is the speed at Daggett

b_{12}, b_{13} are the regression coefficient parameters to be determined from a least squares fit to the data

The preciseness of the fit of the empirical data to the regression equation is measured by the variance of the fit, which is the mean square difference of the measured values of the dependent variables and the simultaneous values computed from Eq. (47).

The analysis was initially performed for a set of monthly averages of speeds recorded at the three sites. For the Mars site, the data base of monthly averages consisting of about 25 months at the 46-m (150-ft) anemometer was extended by using the power law formula to develop equivalent speeds for the 15-m (50-ft) and 91-m (300-ft) anemometers referred to the 46-m height. This added approximately 20 more monthly averages to the regression data.

The results of this regression analysis were disappointing because of a large variance of the fit producing a coefficient of variation equal to 0.21. Upon examining these results it was evident that several of the monthly average speeds were extremely far from the regression equation, with discrepancy ratios of over 50%. Six sets of monthly data were regarded as outliers and removed. Repetition of the analysis for the remaining 41-month set of data reduced the coefficient of variation to 0.17. This, although smaller, is still considered to be large. Furthermore, in some cases the regression coefficients lead to speed predictions that produce inconsistent relative magnitude, so the speeds from measurement and from the regression equation are plotted for comparison in Fig. 15. To test the regression procedure there was an auxiliary analysis performed to consider a single regression problem for the speed at Edwards as a function of the speed at Daggett. Here the fit appeared to be better, with a coefficient of variation of about 0.09. These regression results are plotted on Fig. 16.

Comparison of the obviously greater differences between the measured data and the regression line data in Fig. 15 than in Fig. 16 led to a third repooling of the Mars data, reducing the 41 sets of data into seven larger sets. With this small set of seven points, but many more measurements associated with each point, the multiple regression analysis led to a coefficient of variation of 0.08. Beyond this, a single regression analysis was performed using the Edwards data only, omitting Daggett. The coefficient of variation
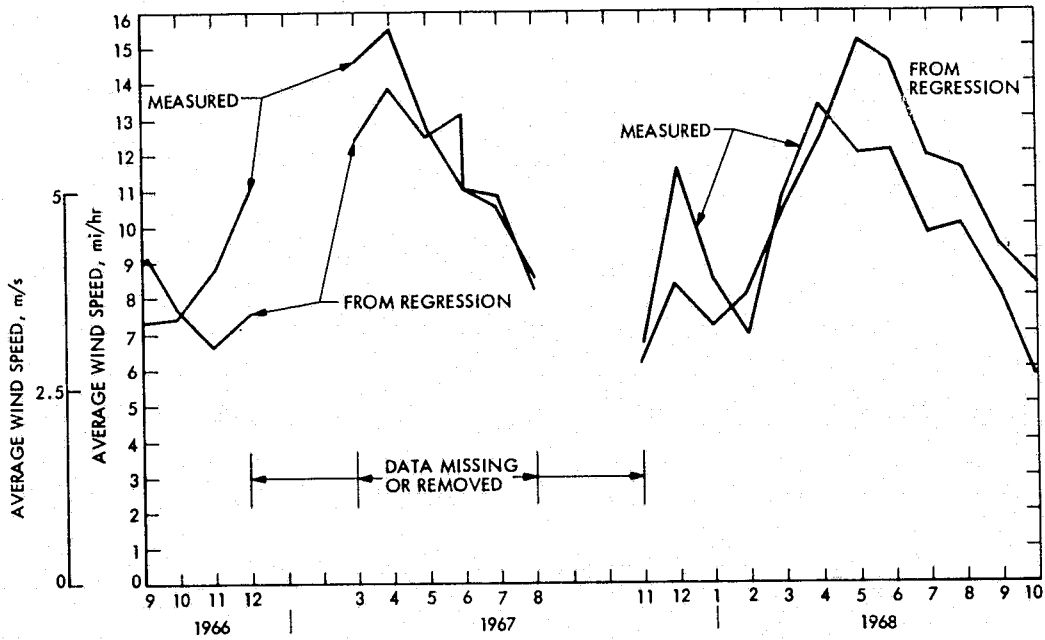
Fig. 15. Mars site average speed regression on Edwards and Daggett
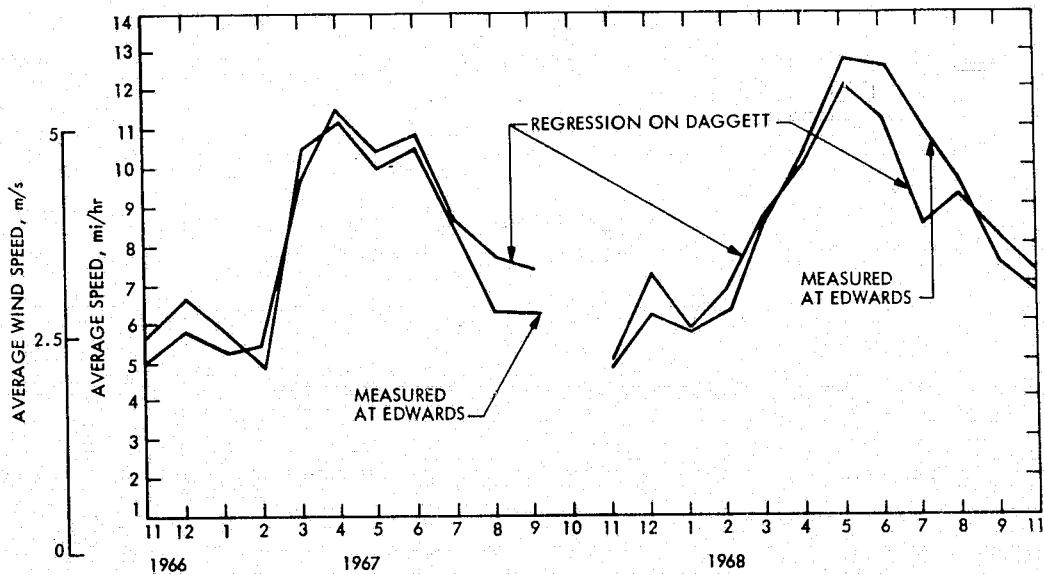
Fig. 16. Edwards wind speed regression on Daggett

Table 10. Regression of Mars site pooled data on Edwards data

Set number	Description	No. of points	Measured speed, mph	Speed from regression	Difference
1	1966: meas. at 50´ convert to 150´	2272	8.563	8.098	−0.47
2	1967: meas. at 50´ convert to 150´	1355	12.556	12.176	−0.38
3	1966: 150´ data	2247	8.253	8.095	−0.16
4	1967: 150´ data	2378	11.185	9.931	−1.25
5	1968: 150´ data	5395	·9.692	11.410	1.72
6	1966: meas. at 300´ convert to 150´	1949	8.897	7.995	−0.90
7	1967: meas. at 300´ convert to 150´	1382	11.431	12.232	0.80

was about 0.11. These results are shown in Table 10 and the regression equation is simplified to

$$x_1 = b_{12} \, x_2 \qquad (48)$$

where the coefficient b_{12} was found to be 1.287. Using this last result, and the computed 14-year average speed at the 4-m anemometer height for the Edwards data of 3.76 m/s (8.41 mi/hr), the prediction of the long-term average speed at the 46-m (150-ft) Mars anemometer is

$$x_1 = 1.287 \times 3.76 = 4.84 \text{ m/s (10.8 mi/hr)}$$

    (2)   <u>Correlation Analysis</u>. In this approach, the long-term mean speed at the Mars site is estimated by

$$x_1 = A + \hat{\rho}\hat{R} \, (C-B) \qquad (49)$$

where

    A is the observed mean speed at the Mars site

    C is the long-term (14 years) observed mean speed at Edwards

    B is the mean speed at Edwards for the same contemporary periods as for A.

    $\hat{\rho}$ is the sample correlation coefficient determined from the data used to find A and B.

    $\hat{R}$ is the ratio of the contemporary standard deviations for the Mars and the Edwards data.

Equation (49) is equivalent to correcting the observations at the Mars site by adjusting for the difference in the Edwards contemporary data with respect to the Edwards long-term data. The contemporary data was defined as the 10 months during the 1966-68 records for which there were two independent readings for each month at the Mars site 46-m anemometer. The sample correlation coefficient and standard deviations were computed from the 10 sets of monthly differences of average speeds at the two locations.

The following factors were determined from analysis of the data:

    $\hat{\rho}$ = 0.523

Sample standard deviations

    Mars site = 2.25

    Edwards = 1.71

    R = 2.25/1.71 = 1.32

    A = 4.45 m/s (10.16 mi/hr)

B = 3.74 m/s (8.38 mi/hr)

C = 3.76 m/s (8.41 mi/hr)

Consequently the long-term average speed estimated for the 46-m anemometer at Mars is

$$x_1 = 4.54 + 0.523 \times 1.32 \quad (3.76-3.74)$$

$$= 4.55 \text{ m/s} = 10.18 \text{ mi/hr}$$

Note that this estimate is similar to, but somewhat less than the estimate obtained from the regression coefficient. However, the latter used data from the remaining two anemometers at the Mars site and scaled these to the 46-m height by means of the power law. In spite of this difference in the data used, the agreement of these results, which were obtained by independent approaches, is within 0.3 m/s. It would also seem logical to estimate the wind speed as somewhere between these two values, say 4.7 m/s (10.5 mi/hr).

     d.   <u>Average Speeds at Additional Goldstone Sites</u>. The additional set of anemometer sites (see Fig. 1) was proposed as useful for exploring candidate locations for windmills. The mean speed at a new site is estimated to be the product of the long-term mean speed at site 001 and the ratio of short-term mean speeds between the new site and site 001.

     To obtain reasonable speed ratios, much more data would have to be processed beyond the limited amount that has been reduced to date. However, we will attempt to use the limited amount of reduced data to make qualitative predictions of the speed ratios for these sites with respect to the 46-m anemometer Mars site speed.

     An ideal approach to obtaining the speed ratios would include a way of accounting for the effect of local terrain on wind speed. A family of isotachs (line of constant wind speed) covering the region of concern would be a convenient way of presenting such information and would permit the selection of best sites for windmills. There are computer programs capable of solving the pertinent equations of fluid motion together with approximations to their boundary and initial conditions so as to produce theoretically constructed isotachs of reasonable accuracy. Representing the boundary conditions for a terrain of valleys and mountains can be very costly if a fine grid of rectangular cells is necessary to give satisfactory resolution. A cursory attempt was made to develop a family of isotachs for the Goldstone area by a subcontractor to MRI (Systems, Science and Software of La Jolla, California). Their method ("STUFF") is described in the MRI Technical Report MRI FR-1260, Oct. 1974. Briefly it consists of representing the flow region with an array of rectangular cells, prescribing a uniform horizontal flow field at the upstream edge of the region, invoking the principles of conservation of mass, momentum, and energy and solving for the velocity components at the center of each cell. Contour maps of the area were used to produce obstacle cells simulating the various hills. A total of 2574 rectangular cells were used, each being 1250 m long by 1250 m wide by 125 m high. This size cell was necessary to keep the cost within the budget. It was a crude representation since several of the hills are smaller than a single cell, yet it was hoped that it might yield useful isotachs.

Figures 17 and 18 show the isotachs obtained for upstream uniform flow fields of 6.0 and 12.0 m/s respectively, both directed from the southwest. The accuracy of the relative speeds between certain points within the region can be checked by comparing the isotach relative speeds to measured ones. Speed and direction data have been collected for the additional sites during the period Oct. 1974 to Jan. 1976. The small amount of this data that has been reduced to usable forms is, nevertheless, enough to test the isotach accuracy. In Table 11 are listed simultaneous speed ratios between the anemometer sites and site 001, the reference site near the Goldstone Mars Station. First, the wind direction record at site 001 was examined for the period Oct. 21 to 30, 1974, and portions of the record were selected where the direction was fairly constant over a period of from 0.75 to 12.00 hours. These time periods and the azimuth wind directions are listed respectively in columns 2 and 3. Within each time period a smaller time interval was found over which both speed signals being compared were fairly constant. In this way the speeds were being compared under apparent steady-state conditions. Two facts are clear: namely, these simultaneous ratios for a given wind direction at site 001 vary considerably, and the ratios for some sites are much higher than for others. For example, except for two entries, all the 003/001 ratios are less than unity, whereas for site 002 all the ratios, except seven, are greater than unity.

In Table 12, the speed ratios from the calculated isotachs are compared to ratios of averaged speed over various time periods. The isotach ratios appear in the first row. The second row contains the ratios of averaged speeds, each of which is based on the 78 datum points. All datum points had wind directions between 180 and 270 deg at site 001. Since the isotach calculations were based upon an upstream flow field coming from azimuth 225 deg, the entries of the second row represent the best comparison to the isotach ratios. The conditions for the other rows are explained in the table.

It is obvious that the correlation between the calculated and measured ratios is poor. This is possible because of a lack of sufficient fineness in the rectangular grid representation of the terrain. It is also clear that the measured speed ratios vary considerably even when the average speed and direction at the reference site are constant. This suggests that the flow field over the area cannot be characterized by the wind velocity at the reference site. Establishment of a representative ratio for a particular site will require the reduction of much more data. An obvious conclusion that follows an examination of Tables 11 and 12 is that certain sites average considerably more wind than others. The average ratios of Table 12 invariably show that sites 002, 005, and 006 have more wind than sites 001, 003, and 004, since this is true for 23 out of 28 cases. It is not surprising that these apparently better sites are hilltops whereas the others are flats.

C.   EXAMPLE POWER ESTIMATE

In considering possible Goldstone windmill sites, one essential requirement is to avoid interference with antenna transmission and reception. Another preferential requirement is that, to reduce proportionate costs of site preparation, access road construction and power transmission, a candidate site should be large enough to accommodate a number of windmills. In addition to these considerations, the candidate sites should also be expected to experience relatively high winds.
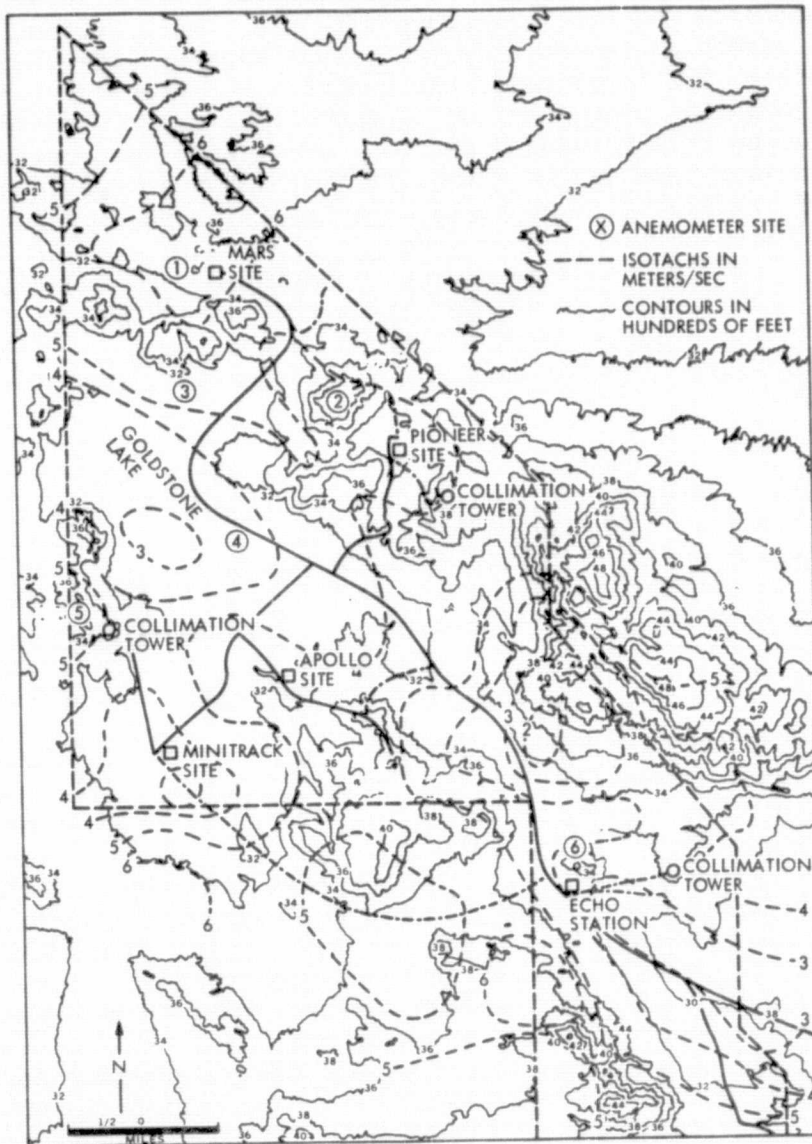
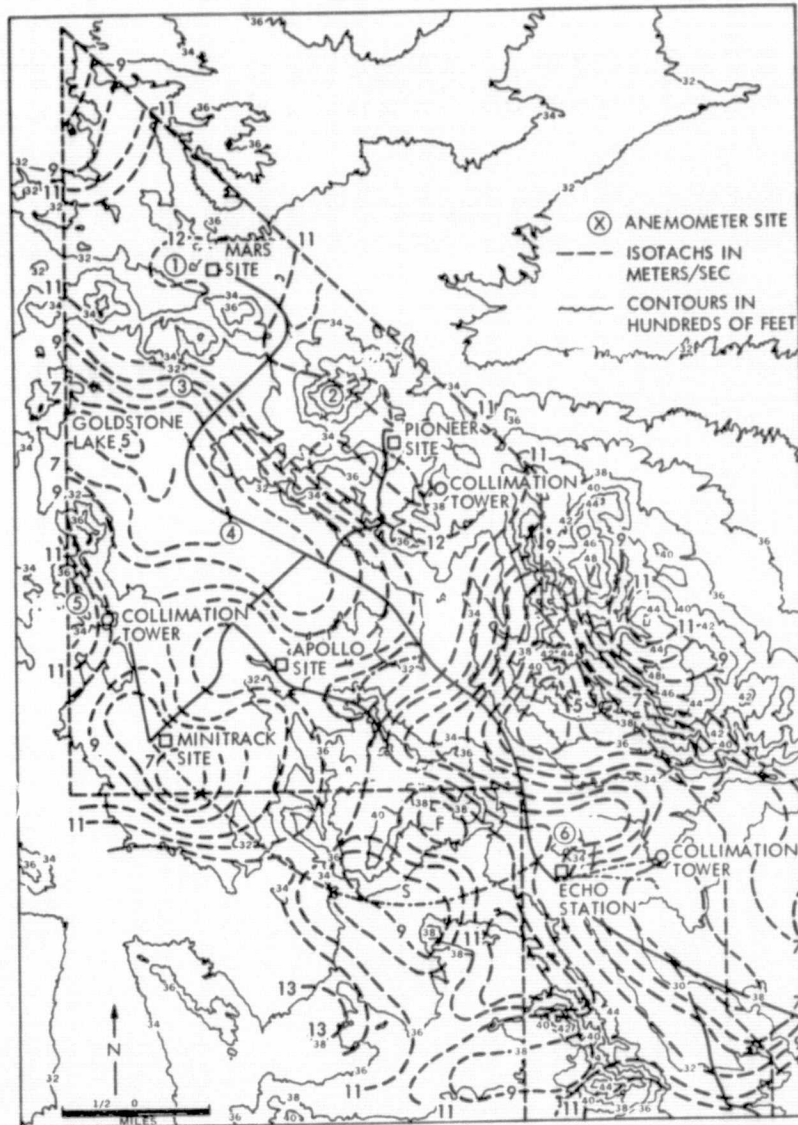Fig. 17. STUFF model isotach analysis of the
median wind speeds

Fig. 18. STUFF model isotach analysis of the
84th percentile wind speeds

Table 11. Simultaneous speed ratios between additional Goldstone sites and reference site

Date, 1974	Length of time period, hr	Wind direction at ref site 001, in deg	Western Ridge, 005 001	Billboard, 002 001	Echo, 006 001	Airport, 004 001	WV, 003 001	Approx windspeed at ref site 001, m/s
10/22	1.25	0	--	1.32	1.58	0.84	0.00	2.24
10/30	3.0	90	--	1.32	0.74	0.58	0.53	4.47
10/26	0.75	90	--	0.53	1.27	1.05	0.91	3.13
10/25	2.0	90	1.27	1.69	0.71	0.63	0.00	3.13
10/25	4.0	90	1.44	1.87	1.53	0.65	0.00	3.58
10/22	2.5	90	1.05	1.05	0.95	0.53	0.79	5.36
10/30	1.0	120	--	1.05	0.74	--	0.64	4.02
10/24	3.0	120	0.94	1.29	1.40	0.65	0.00	3.58
10/24	3.0	120	1.30	1.05	1.14	0.99	0.67	6.26
10/23	2.0	120	0.57	0.96	1.05	0.40	0.28	4.91
10/25	8.0	130	1.39	1.90	0.95	0.98	0.84	6.70
10/24	4.0	130	0.98	0.99	0.71	0.84	0.88	6.70
10/23	2.5	150	--	1.58	0.94	0.26	0.00	3.13
10/23	2.5	180	1.45	1.17	1.17	0.74	0.75	3.13
10/22	3.0	180	1.40	1.93	1.14	1.58	0.65	3.58
10/22	6.0	180	1.32	1.67	1.22	1.05	0.90	8.94
10/21	3.0	200	0.95	0.84	0.88	0.71	0.65	5.81
10/29	4.0	210	--	0.99	1.40	0.98	0.71	6.71
10/26	4.0	210	1.21	0.93	1.55	0.71	0.65	7.60
10/23	4.0	210	1.05	1.29	1.67	0.88	1.18	5.81
10/21	3.8	210	--	1.05	1.24	0.62	0.86	7.60
10/27	3.0	220	1.58	1.43	1.60	0.58	0.37	10.28
10/21	1.0	220	1.34	1.05	1.19	0.71	0.50	6.70
10/29	1.5	240	1.20	0.93	0.93	0.80	0.93	7.60
10/28	3.0	240	--	1.41	1.27	0.91	1.13	13.41
10/28	12.0	270	1.52	1.30	1.22	0.88	0.93	11.16
10/30	2.5	330	--	1.47	1.47	1.05	0.63	2.24
10/29	3.0	330	--	0.67	1.17	0.74	0.63	4.47

All entries are for condition of steady wind direction at reference site 001. All speeds from which ratios are formed were nearly constant. Data taken Oct. 21 to 30, 1974.

Table 12. Average speed ratios from isotachs and measurements at additional Goldstone sites

	Date	Average speed at site 001 in m/s	Ref. site 001	Site 002	Site 003	Site 004	Site 005	Site 006	No. of hourly datum points
Theoretically constructed isotachs. Wind from southwest		12	1.00	0.915	0.875	0.583	1.00	0.750	
Wind direction at site 001 between 180° and 270°	Oct 30-Nov 8, 1974	5.18	1.00	1.46	0.718	0.840	1.34	1.40	78
Wind direction at site 001 from all quadrants	Oct 30-Nov 8, 1974	4.07	1.00	1.35	0.572	0.710	1.16	1.38	240
	Feb 20, 1975	5.93 (3.16)	1.00	1.495	1.23	1.32		2.12	24
	Feb 22, 1975	4.24 (3.24)	1.00	1.93	1.33	1.04		1.54	24
	Feb 25, Feb 26, 1975	1.73 (0.96)	1.00	2.05	0.876	1.04	1.61	1.64	48
	Feb 28, 1975	2.15 (1.15)	1.00	1.72		0.927	1.29	1.36	24
	Mar 1, 1975	4.47 (3.09)	1.00	1.625	1.06	1.07			24
Weighted average of last six rows			1.00	1.52	0.739	0.846	1.24	1.47	

$$\text{Ratio} = \frac{\text{averaged speed at site}}{\text{averaged speed at ref. site 001}}.$$

All ratios have been adjusted to 46-m above ground. Parenthetical numbers below average speed at ref site 001 are the standard deviations

There are two sites at Goldstone that meet the first two of these require-ments. One of these is near anemometer site 003 and the other is a small mesa 3000 meters northwest of and at the same elevation as site 006. If we assume that the wind at this mesa will be about the same as the wind at site 006, Table 12 shows that the speed ratios are about twice as large as those at site 003. Consequently, since this mesa can accommodate as many as nine 25-m-diameter windmills (spaced at 10 diameters apart to prevent airstream interference), this seems to be the best of all the additional Goldstone anemometer sites, and an estimate will be made for the available wind power at this mesa for a 25-m-diameter windmill.

It was shown previously that the predicted long-term average wind speed at the Mars reference site (site 001) is about 4.7 m/s. From Table 12 the wind speed at site 006 had an average ratio of 1.47 to the speed at the refer-ence. With this ratio, the speed at site 006 is estimated at 6.9 m/s. However, the ratio was computed by adjusting to a 46-m elevation. For a windmill diameter of about 25 m, the center would possibly be about 20 m above ground. Consequently, the power law equation can be used to compute the average speed at this site, 20 m above ground, as

$$m = 6.9 \ (20/46)^{0.1405} = 6.1 \ m/s$$

With a shutdown speed of 2-1/2 times this, or 15.25 m/s, Table 7 shows the average pattern factor S_3 for $\beta = 2.5$ to be 2.05. With the previous estimate of air density at Goldstone of $\rho = 1.062$ kg/m^3, Eq. (30a) provides the average annual incident power per unit area as

$$P_A = (1/2)\rho m^3 \ S_3$$

$$= 1/2 \times 1.062 \times 6.1^3 \times 2.05$$

$$= 247 \ W/m^2$$

In the above calculation, an adjustment for turbulence has been omitted. Assuming an aerodynamic efficiency of 30%, the average power input to the generator would be

$$247 \times \pi/4 \times 25^2 \times 0.30 = 36,385 \ W$$

This is about 3.2 times the power (1.47^3) of a windmill placed at the reference site. The required maximum generator capacity at shutdown would be β_3/S_3 times this, or about 277,415 W.

IV. INTERIM MODEL FOR WIND SPEED SIMULATION

A. GENERAL

This discussion is a summary of work previously reported in Ref. 12 that describes in more detail the data analysis and estimation procedures used to establish sample annual records of Goldstone hourly average windspeeds. These wind speed records are established to provide input for the SENSMOD (Ref. 13) energy analysis program, which is being developed as part of the Goldstone Energy System Project. The objective is to determine 12 probability distributions of wind speeds, one for each calendar month. The developed distribution for any particular month is to be a representation of the historical speed distribution for that month at the Goldstone site. Samples can then be generated from these 12 distributions to yield independent measurements on an hourly basis, and combined to yield "sample years" of wind speed data. No requirement was imposed to model the correlations of successive hourly measurements, which would have imposed a substantial additional program. Consequently, with the present simplification, the distributions of wind speeds are not representative of time intervals shorter than one month.

The form of the distribution function of wind speeds s for a given month was assumed to be the modified exponential distribution of Eq. (19), which is repeated here for reference:

$$F(s) = 1-\exp\left[-(as+bs^2)\right], \quad s \geq 0 \tag{50}$$

where a and b are positive parameters characteristic of the month. Thus, for the ith month (i = 1, ..., 12), two parameters, a_i and b_i, are to be determined. This form of distribution has been found to provide good fits for the available data sets, as discussed previously in Section II-C.

The data base consisted of the following three groups of wind speed records, which are subsets of wind records in Tables 1 and 2.

Set	Location	Anemometer height, m(ft)	Period of record, yr/mo to yr/mo	No. of entries
A	Goldstone, Mars site	46(150)	66/11 - 68/10	9100
B	Edwards AFB	4(13)	66/11 - 68/10	17,500
C	Edwards AFB	4(13)	57/1 - 70/12	122,700

Since the actual data for Goldstone, set A, covers a period of less than two years, it is not necessarily a reliable basis for the desired probability models. As a means of assuring that the models represent long-term Goldstone

phenomena, the following steps were taken which are shown on the flow chart of Fig. 19, incorporating data sets B and C into the analysis.

(1) Using a chi-square criterion for goodness of fit, 12 sets (a_i, b_i,) of monthly parameters were chosen based on the A data.

(2) Using data sets A and B, the degree of correlation between monthly wind power (= $E[s^3]$) at Goldstone and Edwards was estimated.

(3) Based on the results of step 2, the long-term data set C from Edwards was used together with A and B to obtain "corrections" of the parameter values found in step 1; the corrected values being designed to incorporate the long-term information provided by set C.

(4) Hourly wind samples were generated using the corrected values of the a_i, b_i parameters for the corresponding months.

B.   COMPUTATION METHODS

1.   <u>Long Term Distribution Function Parameters</u>

<u>Step 1</u>. Fitting parameters to empirical data was performed in two sub-steps. A preliminary regression analysis step was executed to provide class boundaries and starting points for a final chi-square step.

<u>Substep 1</u>. <u>Preliminary Regression Estimate for Parameters a, b of a Sample</u>. By taking the logarithm of both sides of Eq. (50) and rearranging, we have

$$(a + bs) = - \frac{\ln[1-F(s)]}{s}$$

then let $Y_i = a + bs_i$ be the model equation for regression analysis of Y on s, and let

$$\frac{\ln[1-F(s_i)]}{s_i}$$

be the observed values of Y_i, where $F(s_i)$ is the empirical distribution function of s. When recast in this form, a standard linear regression analysis can be used to find the a and b parameters.

<u>Substep 2</u>. <u>Final Chi-Square Calculation Estimate for Parameters a, b of a Sample</u>. Divide the speed range between XMIN and XMAX into 8 interior classes and add one class at the low end to include all speeds below XMIN and one class at the high end to include all speeds above XMAX. Here, XMIN is the threshold wind speed and XMAX is the cutoff speed for power generation, and was taken to be 5 and 35 mph, respectively.
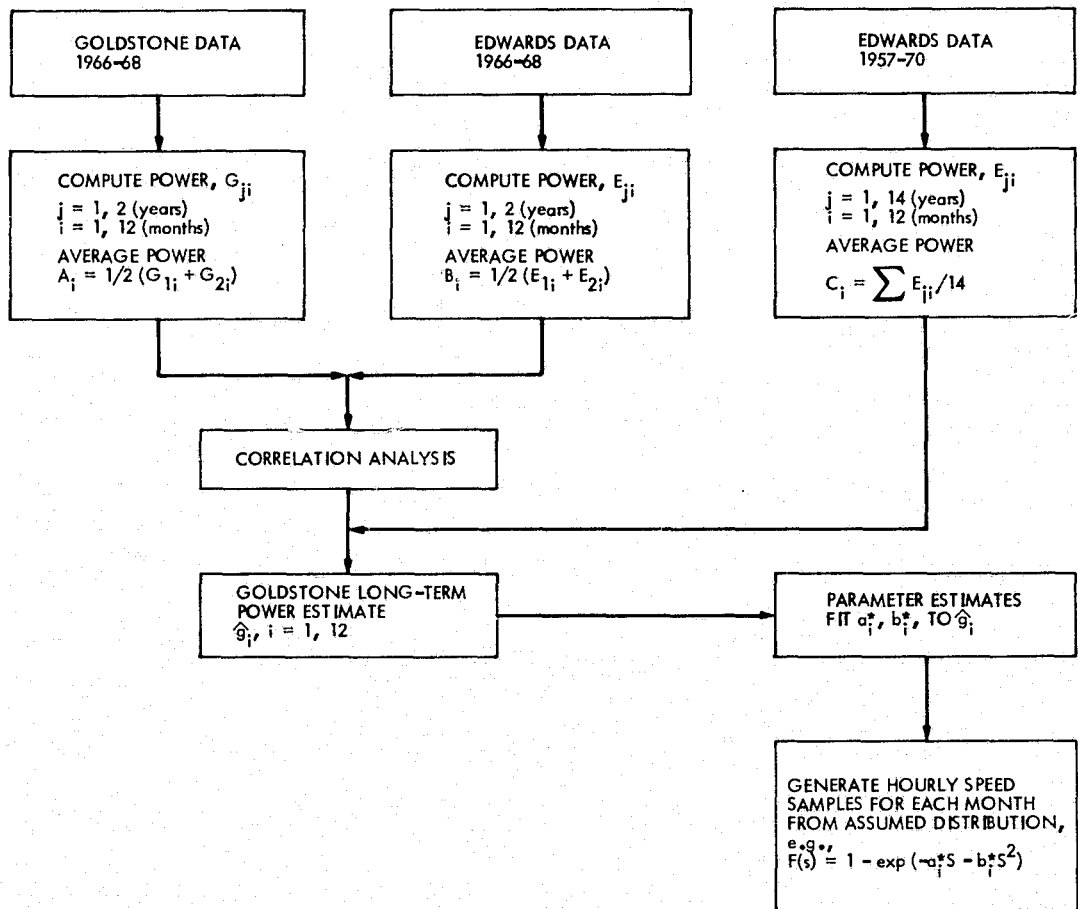
Fig. 19. Goldstone wind speed model for SENSMOD program

Let

    O_j = observed number of speeds in class "j" (from the empirical sample)

    NT = number of observations in the sample

    E_j = expected number in class "j"

Let

    B_j = lower speed class boundary for class "j", then

$$E_j = NT * [F(B_j+1) - F(B_j)]$$

where F(.) is found by evaluating Eq. (50) using the current estimates of a and b. Then the chi-square measure is

$$FUNCT(a,b) = (O_j - E_j)^2 / E_j$$

$$j = 1, 2, \ldots 10$$

The estimate of a and b is made by choosing a, b to minimize FUNCT(a,b). Details of the procedure are described in Ref. 12.

    Step 2. The correlation between data sets A and B was analyzed in terms of wind power P_ρ, defined as a summation of min $[s,25]^3$ (=min $[s^3,25^3]$), where s = wind speed in miles per hour. It is assumed that the true correlation ρ between total power at Goldstone and Edwards in contemporary months is chronologically invariant. It is also assumed that the pair (Goldstone monthly power, Edwards monthly power) has a specific distribution for each calendar month, so that for any specified month the result for any given year is an independent sample from this distribution. It follows from these assumptions that ρ is also the (true) correlation of the pairs of differences. The latter are denoted as follows:

$$(G_{1i} - G_{2i}, E_{1i} - E_{2i}), i = 1, \ldots, 12,$$

where G_{1i} and G_{2i} represent Goldstone power in the ith month of year 1 and year 2, respectively, and E_{1i} and E_{2i} are defined correspondingly for Edwards. Because of missing September and October data at Goldstone, there are only 10 values of i where data from two years are available. These were used to estimate ρ by computation of the sample correlation coefficient of these 10 pairs, yielding the estimate

$$\hat{\rho} = 0.486$$

This correlation coefficient appears to be sufficiently large to confirm that the approach outlined is reasonable; e.g., there is a statistical connection between the random deviations from monthly norms at the two locations, Goldstone and Edwards. (Note, when using the average wind speeds at these sites, the correlation coefficient on the average speeds, rather than power, was found to be 0.523. See Section III-B-3.)

For the analysis that will be described in step 3 below, it is necessary also to estimate the ratio of the standard deviations of G_i and E_i, which are the monthly powers for the ith month. This ratio is assumed to be independent of i and was estimated by the ratio of the two sample standard deviations that are determined for the 10 values of $G_{1i} - G_{2i}$, and for the 10 values of $E_{1i} - E_{2i}$. The result was the estimate $\hat{R}$ of the ratio of standard deviations given by

$$\hat{R} = \sigma_G/\sigma_E = 953/664 = 1.44$$

Step 3. To determine "corrected" (a_i, b_i) pairs, it is necessary first to utilize the correlation information in a rational way. The approach adopted was the following:

(a) Estimate the long-term average of the Goldstone total power for the ith month, for i = 1, ..., 12.

(b) Use the results of (a) to correct the values of a_i and b_i obtained by the chi-square fit in step 1.

To obtain the long-term Goldstone power for i = 1, ..., 12, let

g_i = true mean total power for the ith month (Goldstone)

A_i = average of G_{1i} and G_{2i} (data set A, Table 1, Col. 4)

B_i = average of E_{1i} and E_{2i} (data set B, Table 2, Col. 6)

C_i = average of E_{1i}, ..., E_{14i} (data set C, 14 yrs, Table 2, Col. 7)

(For September and October, A_i and B_i were based on only one months record, not two.)

The estimate used for g_i was of the same form as Eq. (49), which was used for average wind speeds; e.g.,

$$\hat{g}_i = A_i + \hat{\rho}\hat{R} \; (C_i - B_i) \tag{51}$$

The values of A_i, B_i, C_i and g_i are shown in columns 4, 2, 3 and 5, respectively, of Table 13. By the results of step 2

$$\hat{\rho}\hat{R} = 0.486 \times 1.44 = 0.7$$

Equation (51) defines the appropriate "least weighted squares" estimator of g_i in terms of the available data, A_i, B_i, and C_i. This interpretation depends on the correlation ρ and the standard deviation ratio R being known. Using estimates instead, as we have done, is natural and reasonable. More exact analysis is not feasible without knowledge of the form of the joint density functions describing wind at Goldstone and Edwards. (Note that the effect of Eq. (51) is to correct the direct estimate, A_i, of Goldstone wind power by adjusting for the difference between Edwards short-term power in the contemporary period and the long-term power.)

Table 13. Mars site long-term projected parameters

| ① | P_f = Power term | | | | Speed Factor | Long-term parameters | |
| | Edwards | | Goldstone | | | | |
①	② 66-68	③ 57-70	④ 66-68	⑤ Projected	⑥ $\underline{c}$	⑦ $\underline{a}$	⑧ $\underline{b}$
Jan	1045	1101	2856	2895	1.0575	0.08442	0.00068
Feb	1018	1477	2111	2432	1.2581	0.07997	0.00158
Mar	2325	2453	4258	4348	1.0776	0.04506	0.00146
Apr	2792	2814	4801	4817	1.0220	0.02500	0.00223
May	3124	3377	3782	3959	1.0303	0.03333	0.00245
Jun	3064	3179	3158	3239	0.9911	0.02363	0.00377
Jul	2058	2061	1928	1930	0.9650	0.00379	0.00743
Aug	1584	1724	1875	1973	1.00045	0.04339	0.00470
Sep	1538*	1464	1681	1633	0.9711	0.01267	0.00373
Oct	1225*	1211	1088	1078	0.9448	0.15278	0.00061
Nov	750	1088	1803	2404	1.1364	0.09010	0.00104
Dec	1428	960	3365	3037	0.9251	0.08072	0.00072

Having the estimates g_i of Goldstone wind power for the long-term, it is necessary now to use these to correct the a_i and b_i previously obtained. To clarify the method, it is helpful to rewrite Eq. (50) in the form

$$F(s) = 1-\exp\left\{-d\left[\frac{s}{c} + \left(\frac{s}{c}\right)^2\right]\right\}$$

where $c = a/b$ and $d = a^2/b$. Written this way, the family of distribution functions is seen to have a "scale factor" parameter c and a "shape" parameter d. For example, doubling all the wind speeds has the effect of doubling c, leaving d unchanged. On the other hand, if c is held fixed while d is changed, the "shape" changes. The shape effect is that, for very large d, the distribution is close to an exponential distribution, whereas for smaller d, it has thinner tails that are more like those of a normal distribution.

The choice of a distribution to represent the ith month at Goldstone was made as follows: Let $d_i = a_i^2/b_i$ (estimated in step 1) and determine c_i so that the average total power agrees with the value g_i estimated in (a). Thus, a model is chosen which predicts total power in accord with the estimate previously derived and, among all sets of parameters satisfying this restriction, the choice is made to yield the same "shape" as was estimated directly in step 1.

With $a_i{}^*$ and $b_i{}^*$ denoting the parameters of the final distribution chosen for the ith month,

$$a_i{}^* = a_i/c_i$$

$$b_i{}^* = b_i/c_i^2$$

which are shown in columns 7 and 8 of Table 13. The values of the c_i's are shown in column 6. Note that most of the c_i's are close to 1, indicating that the corrections made are small and that the short-term Goldstone data are, on the evidence of sets A, B and C, likely to be representative of the long-term wind parameters at Goldstone.

2. Generation of Sample from the Distribution of Eq. (1)

Step 4. A simulated monthly sample of wind speeds s, sample size N (one per hour), can be constructed from a given distribution by drawing

u_i = uniform (0,1)

i = 1,2,,,N $(28 \times 24 \leq N \leq 31 \times 24)$

and letting

$$s_i = F^{-1}(u_i)$$

where F^{-1} is the inverse distribution function. Using the inverse function of Eq. (1) will provide

$$s_i = \frac{(a^2-4bc)^{1/2}-a}{2b}$$

where

$$c = \ln(u_i)$$

It is a straightforward computer procedure to simulate hourly sample wind speeds by means of the two foregoing relationships.

V. STOCHASTIC WIND SPEED SIMULATION MODEL

A.   FURTHER WORK REQUIRED

A complete energy system comprises windmills, solar energy collectors, energy conversion, and energy storage devices. The performance of such a system depends on how effectively it responds to variable energy demand loading. A prediction of the performance could be obtained through study of a dynamic energy system model that incorporates representative simulated samples of wind speeds, insolation, and energy loading. Such a model would also provide useful design information to establish the appropriate characteristics for the energy generation and storage components, since it can reflect the interactions between the energy that can be produced and the energy demand. This discussion considers simulation of hourly wind speeds, which would be one of the three major stochastic components (wind speed, insolation, demand) of an energy system model.

The preceding discussions have described examinations of many annual records of hourly wind speeds recorded at Goldstone, Edwards Air Force Base, Daggett Marine Center and George Air Force Base. From these we have been able to establish the empirical probability distributions of wind speeds and closed-form functions and the associated parameters that provide good approximations to the empirical distributions. Examinations of these records have led to a convenient method for comparing candidate windmill sites on the basis of expected input annual average power. This method has been shown to provide estimates for a candidate site for which only the average wind speed is known (possibly from existing records) or can be estimated. A monthly wind power model has also been developed and described for a specific Goldstone site via correlation analysis with 14 years of observed Edwards AFB data. This model is designed to give more accurate estimates of the expected monthly power input than would be given by the two years of data available for the Goldstone site.

The work described previously has emphasized examinations of wind speed distributions and average power expected over relatively long periods of time. To extend this work to generate representative hourly wind speed samples as the input to an energy system simulation, it would also be necessary to preserve the statistical characteristics of the hour-to-hour correlation of wind speeds. Much has already been done to establish the nature of the wind speed distribution. On the other hand, relatively little has been performed to establish the correlation functions. Beyond this, new theoretical developments will be required to generate a simulation process that represents both distributions and correlations. As a useful by-product, the simulation process might be adaptable in telemetry noise degradation studies of water vapor in the radar beam path.

B.   THEORETICAL BACKGROUND

In practice, wind speeds have typically and conveniently been characterized as the sum of a slowly changing quasi-steady mean component and a more rapidly changing turbulent component. The mean component is known to be nongaussian, nonzero, with predominating spectra at periods of hours or days. The turbulent component is estimated to be gaussian, mean zero, with spectra peaking at

periods in the order of seconds or minutes. Because of the importance of gust loading on civil engineering structures, much work has been done and several models have been proposed to represent the spectral density of the turbulent component. Unfortunately, possibly because emphasized interest in wind turbines is mostly recent, little or nothing has been done to describe the spectral density of the mean component, which is by far the more important in considering wind turbines. Here we will consider only simulation of the mean speeds. If desirable, the wind power could be adjusted for the effect of turbulence as described in preceding discussions.

A mathematical process to simulate wind speeds should provide a good fit at least in the (first-order) probability distribution and in the auto-correlation (or equivalently in the spectral density). A major initial effort in developing the process is to identify representative distributions and autocorrelations functions. However, these two factors alone do not uniquely specify the random process with which they are associated. Consequently, another major requirement is to devise a random process which possesses desirable first-order probability distribution and autocorrelation characteristics.

Two possible approaches[3] to the random process appear to be promising with respect to providing valid results and reasonable effort in the execution. These are the filtered Poisson process and the transformed Gaussian process. An alternative approach to the process might be through a Markov chain. This has been used with varying success on other climatological phenomena such as temperature and cloud cover. The Markov method permits many simplifications in developing and exercising the simulation model. However, this implies that the autocorrelation function of the generated data is likely to have an exponentially decaying shape. This implication is a severe restriction on modeling wind. As an illustration example, autocovariance (related to auto-correlation) functions for a January and a July record of hourly wind speeds are shown in Fig. 20. The two curves indicate moderate (January) to strong (July) peaks at approximately 24 hours of lag separation. This apparently diurnal cycle, which in general appears to be most evident during summer months, tends to preclude a Markov model that would exhibit monotonically decaying curves.

1. Filtered Poisson Process

This filtered Poisson process has been used successfully for a wide variety of closely related phenomena. One application has been in the field of earthquake simulation (Ref. 14) where nonstationary gaussian processes have been assembled to match the autocorrelation functions and response spectra of the observed phenomena. Simulation of gaussian processes is well established, and can be accomplished by a number of straightforward methods. More recently (Refs. 15 and 16) the Poisson process has been used to represent the turbulent

---

[3]As suggested by Prof. M. Shinozuka of Columbia University, who has also supplied the material for the following discussion of these approaches.
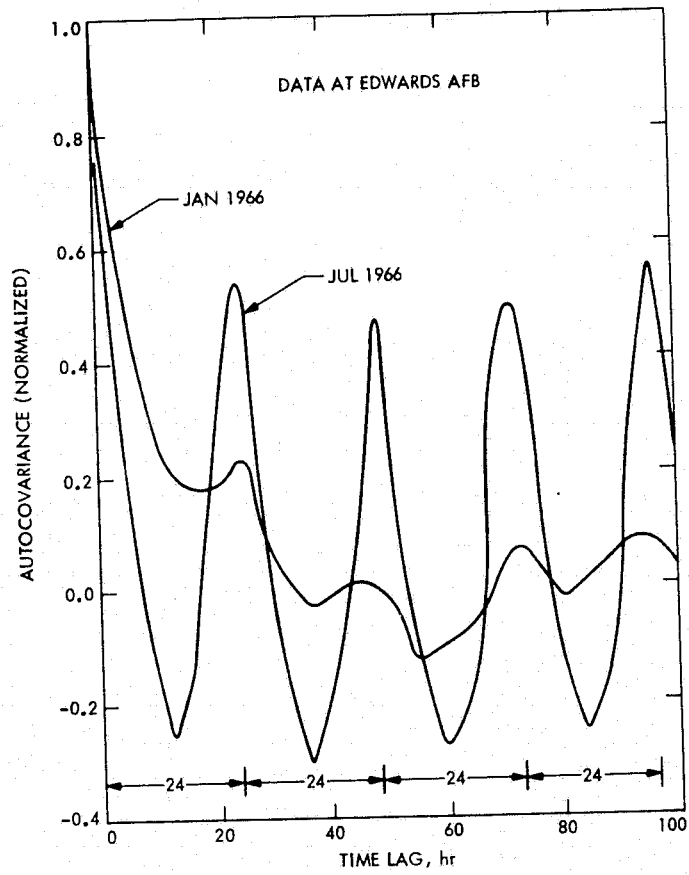
Fig. 20. Examples of autocovariance of
mean wind speeds

component of wind velocity. These wind processes are of particular interest since they describe simulation models that can produce nongaussian distributions such as would be required for the simulation of mean wind speeds. The models described could readily be made to apply through adjustments of parameters.

The essential advantage of using the filtered Poisson process lies in the fact that once a shape pulse function, a distribution function for random pulse amplitude, and Poisson arrival rate are chosen on the basis of data, the characteristic function (or equivalently density function, which is in general nongaussian) as well as the expected value, autocorrelation and spectral density functions can immediately be predicted. Then these functions can be adjusted as necessary to represent the described phenomena to a reasonable degree of accuracy. Furthermore, the generation of the wind speed samples can be accomplished efficiently by digital computer. Reference 16 indicates examples of sample history, probability density functions (theoretical and empirical), power spectral density functions, and other relevant quantities. If necessary, nonstationary filtered Poisson processes can also be constructed and generated in a similar fashion by introducing the time-varying Poisson arrival rate, or by time-dependent envelope functions. Also, the shape, correlation and distribution functions and Poisson arrival rate, may depend on the locality and time of the year. Consequently, a substantial effort could be required to process existing data for the identification and classification of correlations and distributions.

The pseudo-periodic components that are involved in the mean wind speed records representing daily, seasonal, and yearly speed variations can readily be accommodated. Each of these components can be treated as a stationary narrow-band filtered Poisson process centered on a predominant frequency. The observed record can then be interpreted as the sum of the processes, each representing such a filtered Poisson model. An effort must be made to identify appropriate shape functions that will produce such a narrow-band filtered Poisson process. From experience, however, we expect that the use of the impulse response function of a mass-spring-dashpot system as shape function will produce narrow-band filtered Poisson processes. As an alternative, a set of mass-springs in series could be established to make their combined response contain the periodic components.

Decomposition of the observed record into various pseudo-periodic components can be accomplished by means of appropriate moving average techniques, although the required number of points and the time interval between these points to be used in the moving average must be predetermined by trial. In this respect, performing a preliminary spectral analysis on the observed record for the purpose of identifying the predominant frequencies corresponding to these pseudo-periodic components can help to establish the numbers of points and time intervals to extract a particular component.

2.   Transformed Gaussian Process

An additional model, which is more directly related to the gaussian process, could also be investigated. As described and used successfully in Ref. 17, it is possible to construct a nongaussian process $X(t)$ from a gaussian process $Y(t)$ by means of a nonlinear transformation $X(t) = [Y(t)]^m$ in such a way that $X(t)$ at least possesses a specified first-order probability distribution. The spectral density $S_X(\omega)$ of $X(t)$ and the spectral density

$S_Y(\omega)$ of $Y(t)$ are obviously related; $S_Y(\omega)$ can be obtained either analytically or numerically from $S_X(\omega)$. Therefore, a nongaussian process $X(t)$ with the specified first-order probability distribution and with a spectral density approximately equal to the specified can be constructed as long as one can find a zero-memory nonlinear transformation on a gaussian process $Y(t)$ with a known $S_Y(\omega)$ so that $X(t)$ will produce $S_X(\omega)$ as desired. Furthermore, such a nongaussian process $X(t)$ can easily be generated digitally since $Y(t)$ can be generated efficiently with the aid of Fast Fourier Transform techniques.

REFERENCES

1. Putnam, P. C., *Power From the Wind*, D. Van Nostrand Co., Inc., New York, 1948.

2. Kendall & Buckland, *Dictionary of Statistical Terms*, Hafner Publishing Co., New York, 1960, p. 301.

3. Weibull, W., "A Statistical Distribution Function of Wide Applicability," *J. Appl. Mech.*, Sept. 1956, pp. 290-297.

4. Davenport, A. G., "The Dependence of Wind Loads on Meteorological Parameters," Seminar, *Wind Effects on Building Structures*, Ottowa, Canada, Sept. 1967, pp. 19-82.

5. Benjamin, J. R., and Cornell, C. A., *Probability, Statistics, and Decision for Civil Engineers*, McGraw-Hill Book Co., New York, 1970.

6. Golding, E. W., *The Generation of Electricity by Wind Power*, E.&F.N. SPON, Ltd., London, 1955.

7. Sutton, O. G., *Micrometeorology*, McGraw-Hill Book Co., New York, 1953.

8. Simiu, E., "Logarithmic Profiles and Design Wind Speeds," *J. Eng. Mech. Div.*, ASCE, Vol. 99, No. Em5, Proc. Paper 10100, Oct. 1973, pp. 1073-1083.

9. Fiedler, F., and Panafsky, H. A., "Atmospheric Scales and Spectral Caps," *Bull. Am. Meteorol. Soc.*, Vol. 51, No. 12, Dec. 1970, pp. 1114-1119.

10. Davenport, A. G., "The Spectrum of Horizontal Gustiness Near the Ground in High Winds," *Quarterly Journal of the Royal Meteorological Society*, London, Vol. 87, Aug. 1961, pp. 194-211.

11. Hino, M., "Spectrum of Gusty Wind," *Proceedings of the Third Conference on Wind Effects on Buildings and Structures*, Tokyo, Japan, Sept. 6-11, 1971, pp. 69-78.

12. Levy, R., and Lorden, G., "Goldstone Wind Speeds for the SENSMOD Program," *The Deep Space Network Progress Report 42-29*, Jet Propulsion Laboratory, Pasadena, California, Oct. 15, 1975, pp. 141-151.

13. Hamilton, C. C., "A Dynamic Model for Analysis of Solar Energy Systems," *The Deep Space Network Progress Report 42-27*, Jet Propulsion Laboratory, Pasadena, California, June 15, 1975, pp. 41-45.

14. Shinozuka, M., and Sato, Y., "Simulation of Nonstationary Random Processes," *J. Eng. Mech. Div.*, ASCE, Vol. 93, No. 1 Em1, Feb. 1967, pp. 11-40.

15.   Raciot, R., and Moses, F., "Filtered Poisson Process for Random Vibra-
      tion Problems," J. Eng. Mech. Div., ASCE, Vol. 98, No. Em1, Feb. 1972,
      pp. 159-176.

16.   Shinzuka, M., Wai, P., and Vaicaitis, R., "Simulation of a Filtered
      Poisson Process," NSF-GK-37271X1 Technical Report No. 6, Department
      of Civil Engineering and Engineering Mechanics, Columbia University,
      March 1976.

17.   Wilkins, D. J., Wolff, R. V., and Shinozuka, M., "Realism in Fatigue
      Testing: The Effect of Flight by Flight Thermal and Random Load Histories
      on Composite Bonded Joints," ASTM, Special Publication 569, 1975, pp.
      307-377.